Eur. Phys. J. C (2022) 82:561
https://doi.org/10.1140/epjc/s10052-022-10507-6

THE EUROPEAN PHYSICAL JOURNAL C

Check for updates

Regular Article - Theoretical Physics

Muon g − 2, neutralino dark matter and stau NLSP

Mario E. Gómez[1,a], **Qaisar Shafi**[2,b], **Amit Tiwari**[3,c], **Cem Salih Ün**[1,3,d]

[1] Departamento de Ciencias Integradas y Centro de Estudios Avanzados en Física Matemáticas y Computación, Campus del Carmen, Universidad de Huelva, 21071 Huelva, Spain
[2] Department of Physics and Astronomy, University of Delaware, Newark, DE 19716, USA
[3] Department of Physics, Bursa Uludağ University, 16059 Bursa, Turkey

Received: 1 March 2022 / Accepted: 7 June 2022
© The Author(s) 2022

Abstract We explore the implications of resolving the muon $g-2$ anomaly in a $SU(4)_c \times SU(2)_L \times SU(2)_R$ model, where the soft supersymmetry breaking scalar and gaugino masses break the left-right (LR) symmetry. A 2σ resolution of the anomaly requires relatively light sleptons, chargino and LSP neutralino. The stau turns out to be the NLSP of mass $m_{\tilde{\tau}} \lesssim 400$ GeV, and the sleptons from the first two families can be as heavy as about 800 GeV. The chargino is also required to be lighter than about 600 GeV to accommodate the muon $g-2$ solutions consistent with the dark matter relic density constraint. The dominant right-handed nature of the light slepton states suppress the sensitivity of possible signals which can be probed in Run3 experiments at the LHC. We also discuss the impact of accommodating the Higgs boson mass and the vacuum stability of the scalar potential for these solutions. Although a light stau can be compatible with the stability of the scalar potential, the Higgs boson mass constraint has a strong impact on the solutions with $\tan\beta$ bounded from above, namely $\tan\beta \lesssim 20$. The Higgsinos are heavier than about 4 TeV, and the LSP neutralino has the correct relic density if it is Bino-like. We identify stau–neutralino coannihilation as the dominant mechanism for realizing the desired dark matter relic density, with sneutrino–neutralino coannihiliation playing a minor role. These bino-like dark matter solutions can yield a spin-independent scattering cross-section on the order of 10^{-13}pb which hopefully, can be expected to be tested in the near future.

1 Introduction

Supersymmetry (SUSY) is one of the leading candidates for exploring physics beyond the Standard Model (SM) since its minimal version, the minimal Supersymmetric SM (MSSM), provides resolution of some of the fundamental challenges faced by the SM. These include a resolution of the gauge hierarchy problem, presence of non-baryonic dark matter (DM) candidates with the lightest neutral supersymmetric particle (LSP) being stable by R-parity conservation, and stabilization of the electroweak vacuum. In addition, unification of the SM gauge couplings is realized at $M_{\rm GUT} \approx 2 \times 10^{16}$ GeV. The low energy implications of SUSY grand unified theories (GUTs) can be explored in greater detail in experimental observations once the symmetry structure is proposed and the soft supersymmetry breaking (SSB) boundary conditions are imposed at $M_{\rm GUT}$.

SUSY models can also provide a solution to another long standing problem in SM, namely the discrepancy between the theoretical SM calculations and the experimental measurements of the muon anomalous magnetic moment (hereafter muon $g-2$). The FermiLab experiment has recently provided a new experimental value for muon $g-2$, which deviates from the SM prediction by 3.3σ [1]. This discrepancy between the SM prediction and experiment becomes even larger when combined with the earlier measurements at the Brookhaven National Laboratory [2], leading to the following world average in the muon $g-2$ measurements:

$$\Delta a_\mu \equiv a_\mu^{\rm exp} - a_\mu^{\rm SM} = (25.1 \pm 5.9) \times 10^{-10}. \tag{1.1}$$

This new world average points to a 4.2σ deviation from the SM predictions [3–5]. The supersymmetric contributions to muon $g-2$ arise from a number of super partners which couple to muon at tree-level [6–20]. In order to solve this discrepancy, the SUSY electroweak sector should involve relatively light neutralinos, charginos and sleptons. On the other

[a] e-mail: mario.gomez@dfa.uhu.es
[b] e-mail: qshafi@udel.edu
[c] e-mail: amitiit@udel.edu
[d] e-mail: cemsalihun@uludag.edu.tr (corresponding author)

Published online: 25 June 2022

hand, the absence of a direct accelerator signal of SUSY raises the experimental bounds on the sparticle mass spectrum. The lower mass bounds on the colored sparticles currently exclude gluinos and squarks of the first two families lighter than about 2 TeV [21,22]. Despite the relatively lower bounds on the electroweak sector, the sensitivity in the current collider experiments is enough to test chargino masses up to about 1.1 TeV and sleptons to about 350 GeV [23,24]. However, these bounds can be loosened if the lighter sleptons are mostly right-handed [25].

Even though the colored sparticles do not directly contribute to muon $g-2$, the severe bounds on their masses constrain the other particles in SUSY GUTs if universal SSB mass terms are imposed at $M_{\rm GUT}$. For instance, the consistency of Higgs boson mass [26,27] with the experimental measurements requires stops at the TeV scale [28]. Therefore, assigning equal masses to superpartners of the matter fields at $M_{\rm GUT}$ implies an increase in the full mass spectrum.

In this work, we provide a resolution of the muon $g-2$ problem in the framework of supersymmetric $SU(4)_c \times SU(2)_L \times SU(2)_R$ ($4-2-2$, for short), without imposing the discrete LR symmetry on the SSB mass terms. In the scalar sector the SSB mass terms break the LR symmetry but are flavor universal. The paper is organized as follows. We briefly discuss the model and summarize some of its salient features relevant for muon $g-2$ and the current experimental results in Sect. 2. Section 3 describes the scanning procedure after a discussion on the experimental constraints employed in our analyses and their impact on the muon $g-2$ resolution. We present our results for the sparticle spectrum compatible with muon $g-2$ in Sect. 4, and in Sect. 5 we discuss ways to experimentally test the findings in the current and near future DM experiments. We summarize our conclusions in Sect. 6.

2 Model description and muon $g-2$ confronted with Higgs boson

In this section we briefly summarize the supersymmetric $4-2-2$ model [29–31] and some of its salient features. Among the many different breaking schemes of $SO(10)$ [32–38], the $4-2-2$ symmetry can be preserved if $SO(10)$ is broken through the vacuum expectation values (VEVs) of the Higgs fields residing either in 54_H or 210_H Higgs multiplets. Even though both breaking mechanisms result in $4-2-2$, they can be distinguished by the presence or absence of the LR symmetry. The breaking through the VEV in 54_H preserves the so called C-parity [39,40], which transforms the left-handed and right-handed fields into each other. However, if one implements the $SO(10)$ breaking through the 210_H VEV, the C-parity is broken [41]. Note that the SO(10) model involves additional Higgs fields such as 126_H whose VEV breaks $4-2-2$ to the MSSM gauge symmetry. With this $\overline{126}_H$ VEV, the D-term contributions to the SSB mass terms are canceled. Furthermore, an unbroken discrete $\mathcal{Z}_2$ gauge symmetry ensures the stability of the lightest LSP [39].

The breaking of $4-2-2$ to the MSSM gauge group leaves intact the hypercharge generator Y, where

$$Y = \sqrt{\frac{3}{5}} I_{3R} + \sqrt{\frac{2}{5}}(B-L). \tag{2.1}$$

Here I_{3R} and $B-L$ represent the diagonal generators of $SU(2)_R$ and $SU(4)_c$, respectively. Taking into account supersymmetry breaking yields the following relation among the three SSB gaugino masses at the GUT scale:

$$M_1 = \frac{3}{5} M_{2R} + \frac{2}{5} M_4, \tag{2.2}$$

where M_{2R} and M_4 denote the gaugino mass terms for $SU(2)_R$ and $SU(4)_c$, respectively, and $M_3 = M_4$ at $M_{\rm GUT}$. If the LR breaking in the gaugino sector is parametrised as $M_{2R} = y_{LR} M_{2L}$, where M_{2L} is the SSB mass of $SU(2)_L$ gaugino, the SSB gaugino masses become independent. This non-universality in gaugino masses helps to remove the tension between the supersymmetric muon $g-2$ contributions and the fairly severe gluino mass bound.

The broken LR symmetry, in general, implies non-universal masses for the soft left- and right-handed matter scalar masses which can be quantified as $m_R \equiv x_{LR} m_L$, where m_R (m_L) denotes the SSB mass of the right-handed (left-handed) fields. In addition to the gaugino and scalar soft masses, the MSSM Higgs fields are realized as superpositions of the appropriate Higgs fields residing in different representations mentioned in the $SO(10)$ and $4-2-2$ breakings. Hence, the boundary conditions for the SSB mass terms also involve non-universal mass terms for the MSSM Higgs fields.

In our work, we assume that the $4-2-2$ symmetry is broken to the MSSM gauge group near the GUT scale, and thus we require the solutions to approximately maintain unification of the SM gauge couplings at $M_{\rm GUT}$. The $4-2-2$ particle spectrum contains the right-handed neutrinos, and the tiny neutrino masses established by the current experiments [42] require either very heavy right-handed neutrinos or negligible couplings between the MSSM particles and the right-handed neutrinos ($Y_\nu \lesssim 10^{-7}$) [43–45], and so the right-handed neutrinos effectively decouple from the MSSM spectrum. Thus, the model below $M_{\rm GUT}$ turns out to be MSSM. The supersymmetric muon $g-2$ contributions arise from the electroweak sector of MSSM involving the Bino, Wino, Higgsinos and sleptons [46–48], and the leading one-loop diagrams are shown in Fig. 1. The top-left diagram in Fig. 1, involves the Bino and smuons and it represents the dominant contribution to muon $g-2$, which is enhanced by the chirality flip (shown with a cross) between the smuons. The contribution is proportional to $\mu \tan\beta$, where μ rep-

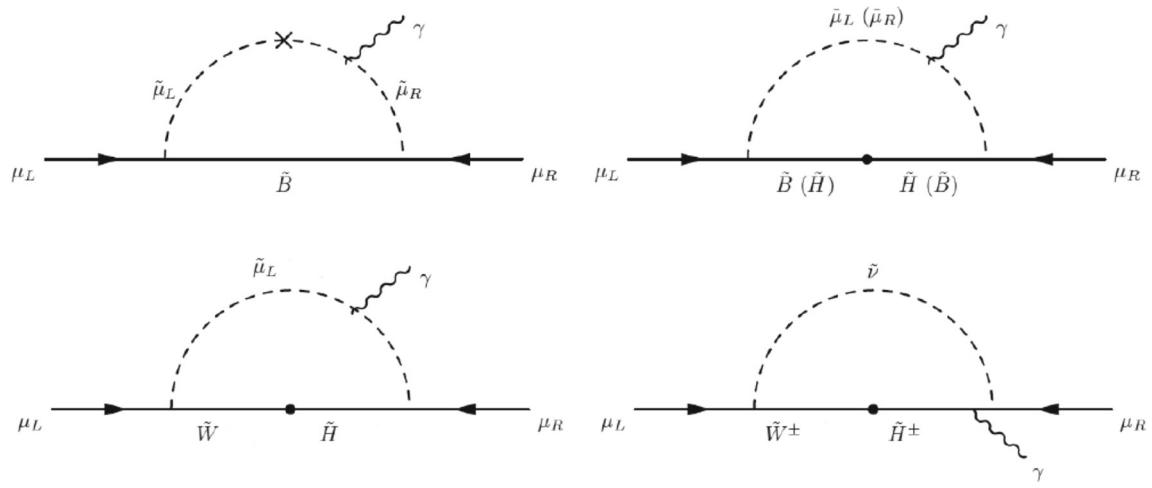


Fig. 1 The leading contributions to the muon $g-2$ through neutralino and chargino loops. The cross in the top-left diagram denotes the chirality flip between the left- and right-handed smuons, while the dots in the other diagrams represent the mixing between different Neutralino species. In the top-right diagram, there is another loop which is formed by the particles given in the parentheses

resents the bilinear mixing term of the MSSM Higgs fields, and $\tan\beta$ is the ratio of their VEVs, $\tan\beta \equiv v_u/v_d$. Thus, the solution of the muon $g-2$ discrepancy favors large $\mu\tan\beta$ values, and the dominant contributions to muon $g-2$ can be calculated approximately as [49]

$$\Delta a_\mu^{\tilde{B}\tilde{\mu}_L\tilde{\mu}_R} \simeq \frac{g_1^2}{16\pi^2}\frac{m_\mu^2 M_{\tilde{B}}(\mu\tan\beta - A_\mu)}{m_{\tilde{\mu}_L}^2 m_{\tilde{\mu}_R}^2} F_N \times \left(\frac{m_{\tilde{\mu}_L}^2}{M_{\tilde{B}}^2}, \frac{m_{\tilde{\mu}_R}^2}{M_{\tilde{B}}^2}\right), \tag{2.3}$$

where

$$F_N(x,y) = xy\left[\frac{-3+x+y+xy}{(x-1)^2(y-1)^2} + \frac{2x\log(x)}{(x-y)(x-1)^3} - \frac{2y\log(y)}{(x-y)(y-1)^3}\right]. \tag{2.4}$$

The remaining diagrams in Fig. 1 also contribute to muon $g-2$ through the mixing of Higgsinos with Bino and Wino, with similar contributions from the sneutrinos. However, these three diagrams are suppressed by the small Yukawa couplings of the lighter generations. In sum, the relevant parameters for this process are listed in Table 1.

We emphasize that the non-universality imposed in the SSB scalar masses is family independent and it distinguishes only the left-handed supersymmetric particles from the right-handed ones. In this context, there exists a tension between the desired muon $g-2$ contributions and the measured SM-like Higgs boson mass. The SUSY spectrum needs relatively heavy third family masses in order to accommodate a Higgs boson mass of about 125 GeV, whereas sizeable contributions to muon $g-2$ favor relatively light sparticles, at least in the

Table 1 The fundamental parameters determining the supersymmetric contributions to muon $g-2$ at the low scale (left) and GUT scale (right)

Low scale	GUT scale
$m_{\tilde{\mu}_L}, m_{\tilde{\nu}}$	m_L
$m_{\tilde{\mu}_R}$	m_R
$M_{\tilde{B}}$	M_1
$M_{\tilde{W}}$	M_{2L}
μ	m_{H_u}, m_{H_d}
A_μ	A_0
$\tan\beta$	$\tan\beta$

electroweak sector. The loop contributions to the Higgs boson mass in the MSSM framework can be written as [50]

$$\Delta m_h^2 \simeq \frac{m_t^4}{16\pi^2 v^2\sin^2\beta}\frac{\mu A_t}{M_{\rm SUSY}^2}\left[\frac{A_t^2}{M_{\rm SUSY}^2} - 6\right] + \frac{y_b^4 v^2}{16\pi^2}\sin^2\beta\frac{\mu^3 A_b}{M_{\rm SUSY}^4} + \frac{y_\tau^4 v^2}{48\pi^2}\sin^2\beta\frac{\mu^3 A_\tau}{m_{\tilde{\tau}}^4}, \tag{2.5}$$

where $M_{\rm SUSY} \equiv \sqrt{m_{\tilde{t}_L} m_{\tilde{t}_R}}$. The first line of Eq. (2.5) represents the contributions from the stops, and the contributions depicted in the second line come from the sbottom and stau, respectively.

The stops contribution is dominant in Eq. (2.5), whereas the contributions from the sbottom and stau can be important for moderate and large $\tan\beta$ values. However, the vacuum stability constraints on $\mu\tan\beta$ [50–52] only allows minor contributions from these terms. Nevertheless, the solutions with moderate or large $\tan\beta$ also yield some suppression in

the contributions from the stop. Thus, such acceptable solutions need heavy stops and/or large trilinear coupling (A_t) to satisfy the Higgs boson mass constraint. On the other hand, as one can see from Eq. (2.3), the solutions with moderate or large $\tan\beta$ can give rise to a parameter space compatible with the muon $g-2$ solution since the supersymmetric contributions are enhanced by $\tan\beta$. Therefore, if family-independent SSB mass terms are imposed at the GUT scale, the sparticles from the first two families become sensitive to the impact from the Higgs boson mass on the third family sparticles. One may have to compromise to accommodate the muon $g-2$ resolution with a consistent Higgs boson mass.

Another tension between the Higgs boson mass and the muon $g-2$ resolution arises if one considers the vacuum stability of the MSSM scalar potential. Resolving muon $g-2$ yields relatively light staus in the spectrum compatible with the Higgs boson mass constraint, but the negative coupling between the Higgs fields and the staus tends to destabilize the vacuum, and the metastability condition on the MSSM scalar potential can have a strong impact for stau masses lighter than about 1 TeV. An overall upper bound from the metastability condition can be expressed as $\mu\tan\beta \lesssim 100$ TeV [50–52], if both the left-handed and right-handed staus are lighter than about 600 GeV. However, this can increase to 700 TeV or so if one of the staus is heavier than about 1 TeV [25]. Hence, one cannot realize arbitrarily large values of μ and $\tan\beta$ to obtain the desired supersymmetric muon $g-2$ contributions.

Indeed, the parameter space compatible with the experimental muon $g-2$ values in SUSY GUTs can lead to μ values up to about 5 TeV or so, even though it is possible to satisfy the vacuum stability constraint with μ as large as 10 TeV. A large value of μ would also imply large values for the other SSB masses in the scalar potential. For instance, the minimization of the scalar potential leads to the relation:

$$\frac{M_Z^2}{2} = \frac{m_{H_d}^2 - m_{H_u}^2\tan\beta}{\tan^2\beta - 1} - \mu^2, \tag{2.6}$$

where m_{H_d} and m_{H_u} are the SSB mass terms for the MSSM Higgs fields, and we assume the loop corrections to be included in these mass terms. Considering the suppression from $\tan\beta$ on $m_{H_d}^2$, Eq. (2.6) can be approximated as $M_Z^2 \approx -2m_{H_u}^2 - 2\mu^2$. Thus, realizing large μ at the low scale requires one to impose either large M_1 and M_2 values, or large m_{H_u} values at the GUT scale. Large M_1 and M_2 values cause a direct suppression in the muon $g-2$ contributions as can be seen from Eqs. (2.3 and 2.4). Similarly, if one inputs a large m_{H_u} value at the GUT scale, it significantly enhances the scalar masses through Renormalization group equations (RGEs) and yields heavy sleptons in the spectrum, which also suppress the muon $g-2$ contributions. Therefore, even though the muon $g-2$ resolution seems to favor large μ and $\tan\beta$ values, it cannot be easily accommodated in SUSY GUTs with large values for μ and $\tan\beta$ due to negative impacts on the Higgs boson mass, vacuum stability and RGE flow.

3 Scanning procedure and experimental constraints

We perform random scans in the fundamental parameter space of $4-2-2$ with broken LR symmetry by using SPheno-4.0.4 [53,54], which is implemented by SARAH-4.14.4 [55,56]. The fundamental parameter space is spanned by the parameters listed as follows:

$$\begin{aligned}
0 \le\ & m_L && \le 5\,\text{TeV}\\
0 \le\ & M_{2L} && \le 5\,\text{TeV}\\
-3 \le\ & M_3 && \le 5\,\text{TeV}\\
-3 \le\ & A_0/m_L && \le 3\\
1.2 \le\ & \tan\beta && \le 60\\
0 \le\ & \mathrm{x_{LR}} && \le 3\\
-3 \le\ & \mathrm{y_{LR}} && \le 3\\
0 \le\ & \mathrm{x_d} && \le 3\\
-1 \le\ & \mathrm{x_u} && \le 2.
\end{aligned} \tag{3.1}$$

Here x_d and x_u parametrise the non-universality in the SSB masses at $M_{\rm GUT}$ of the MSSM Higgs fields as $m_{H_d}^2 = x_d m_L^2$ and $m_{H_u}^2 = x_u m_L^2$. In addition, we vary the universal trilinear scalar interaction term A_0 by requiring that the magnitude of its ratio to m_L is not greater than 3 to avoid the color/charge breaking minima of the scalar potential [57–59]. Note that Eq. (3.1) does not represent all the phenomenologically available parameter space, but it is rather optimized to emphasize the muon $g-2$ impact on the fundamental parameter space, and the ranges are determined based on the discussion in Sect. 2. In scanning the parameter space given in Eq. (3.1) we employed the Metropolis-Hastings algorithm [60,61], and generated the solutions by following flat priors [62].

All solutions in our scans are required to be compatible with the unification condition on the SM gauge couplings at $M_{\rm GUT}$. The SPheno package first runs RGEs for the gauge and Yukawa couplings from M_Z to $M_{\rm GUT}$, which is calculated as a scale at which the unification condition is realized as $g_1 = g_2 \simeq g_3$, and the deviation of g_3 from unification is restricted not to be larger than about 3%. After $M_{\rm GUT}$ is determined, the RGEs are run back from $M_{\rm GUT}$ to M_Z together with the SSB terms determined by the parameters listed in Eq. (3.1). The results after the RGE evolution involve the low scale mass spectrum, mixings, decay channels and their branching ratios. The mass spectrum depicts the loop-corrected masses up to two-loop level. The Higgsino mass, determined by μ^2, can be calculated through the minimisation of the scalar potential, which leads to the relation given in Eq. (2.6). In addition, considering the tadpole equations, one can also calculate B_μ, the SSB counter part of μ^2. After inputting μ^2, B_μ^2, $m_{H_u}^2$ and $m_{H_d}^2$, SPheno cal-

culates the physical masses of the Higgs bosons by rotating the mass-squared matrices. If these parameters are calculated using the tree-level values, then the resulting masses will represent the tree-level masses. SPheno improves the scalar potential by including the tadpole corrections in the minimisation condition of the effective scalar potential at one loop-level [63,64], and by employing the two-loop corrections to $m^2_{H_u}$ and $m^2_{H_d}$ in Eq. (2.6) to calculate μ^2 and B_μ beyond the tree-level [65]. SPheno employs all possible contributions from the self-energy diagrams to the Higgs boson masses. In addition to the one-loop corrections, SPheno considers the leading order two-loop corrections controlled by the top and bottom Yukawa couplings and the strong gauge coupling [65,66]. We should also note that for the calculation of the Standard Model (SM) Higgs boson mass we use the method implemented in SPheno which runs three-loop RGEs by considering the effective SM Higgs potential between M_Z and $M_{\rm SUSY}$ and imposing the two-scale matching condition at $M_{\rm SUSY}$. The SPheno outputs are transferred to micrOMEGAs [67], which calculates the relic density and the scattering cross-sections of the DM candidates.

After generating the data, we successively apply the mass bounds [68] and the constraints from rare B-meson decays [69,70] as well as the current results from the Planck satellite [71] on the relic dark matter density. The constraints from rare B-meson decays yield a strong impact mostly in the MSSM Higgs spectrum. The current experimental results on these decay modes reveal a strong agreement with the SM predictions and so there is little room for new physics contributions. This agreement has been strengthened even further after the observation of $B_s \to \mu^+\mu^-$ [69]. These processes are mediated by the CP-odd Higgs boson in MSSM and their rate is proportional to $\tan^6\beta/m_A^4$ [72,73], and consequently consistency with these experiments requires a heavy CP-odd Higgs boson especially in regions where $\tan\beta$ varies from moderate to large values. Similarly, the constraint on ${\rm BR}(B \to X_s\gamma)$ leads to a strong lower bound on the charged Higgs boson mass, since the leading order contribution to this process involves the latter [74]. Its contribution can easily spoil the strong agreement between the experimental measurements [70] and the SM predictions [75,76] due to its large Yukawa coupling to the top and bottom quarks. In addition, its contribution is further enhanced by $\tan\beta$ [77]. In this context, the supersymmetric contributions should be suppressed either by a small $\tan\beta$ or a considerably heavy charged Higgs boson. In the case of muon $g-2$ solutions, since moderate and/or large $\tan\beta$ is favored, the constraints from $B \to X_s\gamma$ processes yield a strong lower bound on the charged Higgs boson. Indeed, a consistent prediction for ${\rm BR}(B \to X_s\gamma)$ can exclude the solutions with $m_{H^\pm} \lesssim 400$ GeV (see, for instance, [78]).

In order to realize a compatible DM particle in the spectrum, we accept only solutions that yield one of the MSSM neutralinos to be LSP. The DM considerations, following the Planck Satellite measurements, impose severe restrictions on SUSY models with a neutralino DM candidate. Moreover, if the LSP neutralino is mostly Bino-like, models in which the muon $g-2$ problem is resolved typically predict an inconsistently large relic DM density. However, these values become compatible with the Planck satellite measurements in models with the appropriate annihilation and LSP-NLSP (next to LSP) coannihilation channels.

As discussed before, a resolution of the muon $g-2$ problem favors a light mass spectrum for the electroweak sector particles which may yield multiple coannihilation scenarios. In this context, the NLSP and its interactions with the LSP play an important role in the DM phenomenology. It is also possible to realize a Higgsino-like DM neutralino, and in such cases the relic density constraint excludes the LSP mass up to about 700 GeV [79–81]. However, a Higgsino-like DM in this mass range still leads to a scattering cross-section which is beyond the current sensitivity of the direct detection experiments. If one imposes the null results from the direct detection experiments, the lower bound on the Higgsino-like DM is further extended up to about 1.1 TeV [82]. A similar discussion also holds for the Wino-like LSP neutralino. Note that despite the rather precise determination of the DM relic density provided by the Planck satellite, we employ a 5σ uncertainty to compensate for significant theoretical uncertainties in the relic density calculation of the LSP neutralino, which exceed the statistical uncertainties in the experimental measurements [83,84]. We can summarize the experimental constraints employed in our analyses as follows:

$$\begin{gathered} m_h = 123{-}127\,{\rm GeV} \\ m_{\tilde g} \geq 2.1\,{\rm TeV}\ (800\,{\rm GeV\ if\ it\ is\ NLSP}) \\ 0.8\times10^{-9} \leq {\rm BR}(B_s \to \mu^+\mu^-) \leq 6.2\times10^{-9}\ (2\sigma) \\ 2.99\times10^{-4} \leq {\rm BR}(B \to X_s\gamma) \leq 3.87\times10^{-4}\ (2\sigma) \\ 0.114 \leq \Omega_{\rm CDM}h^2 \leq 0.126. \end{gathered} \tag{3.2}$$

Note that although we have listed only the mass bounds on the Higgs boson and gluino because they have been model independently updated by the Large Hadron Collider (LHC) analyses, we employ the model independent bounds such as those from the Linear electron-positron collider (LEP2), which exclude any new charged particle lighter than about 100 GeV. Despite the precise experimental determination of the Higgs boson we allow an uncertainty of about 2 GeV, which accounts for the theoretical uncertainties. We set the top quark mass to its central value ($m_t = 173.3$ GeV [85]). Even though the supersymmetric spectrum is not very sensitive to the top quark mass, 1σ or 2σ variation in its mass together with the uncertainties in the strong gauge coupling yields a 2–3 GeV shift in the SM-like Higgs boson mass [86–88]. The supersymmetric particles yield about 1.5 (0.5) GeV uncertainty in the Higgs boson mass in the case of large (small) stop mixing [63,89–92].

Of course, we require the solutions to be compatible with radiative electroweak symmetry breaking (REWSB), which constrains μ with respect to the SSB mass terms m_{H_u} and m_{H_d} as given in Eq. (2.6). However, these constraints bound only the magnitude of μ and, following most conventions, we assume it to be positive for all the solutions generated in our scans. Note that positive values of μ do not guarantee positive supersymmetric contributions to muon $g-2$ in our setup, since we allow negative values for M_3, which can yield negative M_1 through the gaugino mass relation given in Eq. (2.2). The signs of the Bino and Wino contributions are determined by $\text{sgn}(\mu M_1)$ and $\text{sgn}(\mu M_2)$, respectively, and the overall sign of Δa_μ depends on the particles involved in the dominant contributions. In this context, we require that all the solutions presented in our results do not worsen the SM prediction on Δa_μ by applying the condition $\Delta a_\mu \geq 0$. In addition, μ can be constrained further by the metastability condition on the MSSM scalar potential, which is discussed in Sect. 2. However, these constraints can bound only the magnitude of μ and, following most conventions, we assume it to be positive for all the solutions generated in our scans.

4 Sparticle spectrum and muon g − 2

We first discuss the impact of the muon $g-2$ measurements on the sparticle spectrum. As previously discussed, the supersymmetric muon $g-2$ contributions favor a relatively light spectrum which can be directly seen from the fundamental parameters shown in Fig. 2 with plots in the $\Delta a_\mu - m_L$, $\Delta a_\mu - m_R$, $\Delta a_\mu - M_1$ and $\Delta a_\mu - M_2$ planes. All solutions are compatible with the REWSB and LSP neutralino conditions. The green points are allowed by the mass bounds and constraints from rare B-meson decays. The red points form a subset of green and they satisfy the Planck measurements on the relic density of LSP neutralino within 5σ. The horizontal solid, dashed and dotted lines bound the regions which accommodate the muon $g-2$ solution within $1\sigma, 2\sigma$ and 3σ respectively. The top panels in Fig. 2 reveal a strong impact on the SSB masses for the matter scalars, which mostly restricts m_L to be lighter than about 600 GeV in order to resolve the muon $g-2$ discrepancy within 2σ, whereas m_R can be as heavy as about 1 TeV (green points). If one strictly requires these solutions to satisfy the correct relic density for the LSP neutralino (red points), these bounds are lowered further, namely $m_L \lesssim 400$ GeV and $m_R \lesssim 700$ GeV. A similar impact can also be observed on the SSB gaugino mass terms as shown in the bottom panels of Fig. 2. The mass bounds and constraints from rare B-meson decays (green points) together with the muon $g-2$ solution within 2σ allow M_1 to be as heavy as about 2 TeV, while the Planck measurements on the relic density of the LSP neutralino (red points) lower its bound to about 1 TeV. Our scans also result in a similar bound on M_2, which cannot be heavier than about 1 TeV.

The observed bounds on the input parameters shown in Fig. 2 can be understood in terms of the impact from the muon $g-2$ and DM relic density conditions. The green stripe with $M_{2L} \gtrsim 200$ GeV in the $\Delta a_\mu - M_{2L}$ plane leads to a considerably light Wino in the mass spectrum, and the smuon masses (controlled by m_L and m_R at the GUT scale) can be relatively heavy ($m_L \sim$ 400–600 GeV, $m_R \sim$ 800–1000 GeV), while the values of Δa_μ remain within the 2σ range of the experimental measurements. These solutions simultaneously predict the stau–neutralino and chargino–neutralino coannihilation scenarios, which significantly lower the relic density of LSP neutralino ($\Omega h^2 \sim 10^{-3}$). This interplay among the input terms requires heavier M_{2L} to remove the chargino–neutralino coannihilation scenario when one requires the solutions to yield the desired DM relic density. However, since the heavier M_{2L} slightly suppresses the supersymmetric muon $g-2$ contributions, this suppression needs to be compensated with relatively lighter smuon masses, which can be realized with $m_L \lesssim 400$ GeV and $m_R \lesssim 800$ GeV.

Among these SSB mass parameters, m_R and M_1 are determined through the LR breaking parameters x_{LR} and y_{LR} plotted in the $\Delta a_\mu - x_{LR}$ and $\Delta a_\mu - y_{LR}$ planes of Fig. 3. The meanings of colors and horizontal lines are the same as in Fig. 2. The LR breaking in the scalar sector can be as large as $x_{LR} \simeq 2.7$ consistent with the DM constraint, and the muon $g-2$ solutions favor the regions with $x_{LR} \simeq 0.7-1.1$. On the other hand, the impact of LR breaking in the gaugino sector strongly restricts $y_{LR} \lesssim -2$. Indeed, this arises mostly from the severe bound on the gluino mass, which can be satisfied with $M_3 \gg M_2$. According to Eq. (2.2), a large and negative y_{LR} is required to realize $M_1 \lesssim 1$ TeV and resolve the muon $g-2$ discrepancy to within 2σ.

We display our results for the SSB trilinear scalar interaction term and $\tan\beta$ in the top panels of Fig. 4, with the colors and horizontal lines defined as in Fig. 2. Another impact from the Higgs boson mass constraint can be observed in the $\Delta a_\mu - A_0/m_L$ plane. Since the contributions relevant to A_0 in muon $g-2$ are suppressed by the muon Yukawa coupling ($y_\mu \sim 10^{-3}$), the muon $g-2$ values are nearly insensitive to the values of A_0. On the other hand, since the Higgs boson mass does not receive sufficient radiative contributions from the sbottom and stau, the favored A_0 values can be understood with A_t in the calculation of the Higgs boson mass, which can be seen from the first line of Eq. (2.5). The dominant term in the stop contributions involves $-6A_t$, which, in turn, contributes positively to the Higgs boson mass when A_t (and so A_0) is negative [86]. In this context, the desired muon $g-2$ solution can be realized with $A_0 < 0$. Even though its ratio to m_L can be as small as about 0.2, the relic density results from the Planck satellite require $A_0/m_L \lesssim -1.2$, so that $|A_0| > m_L$. An interesting dependence on the super-

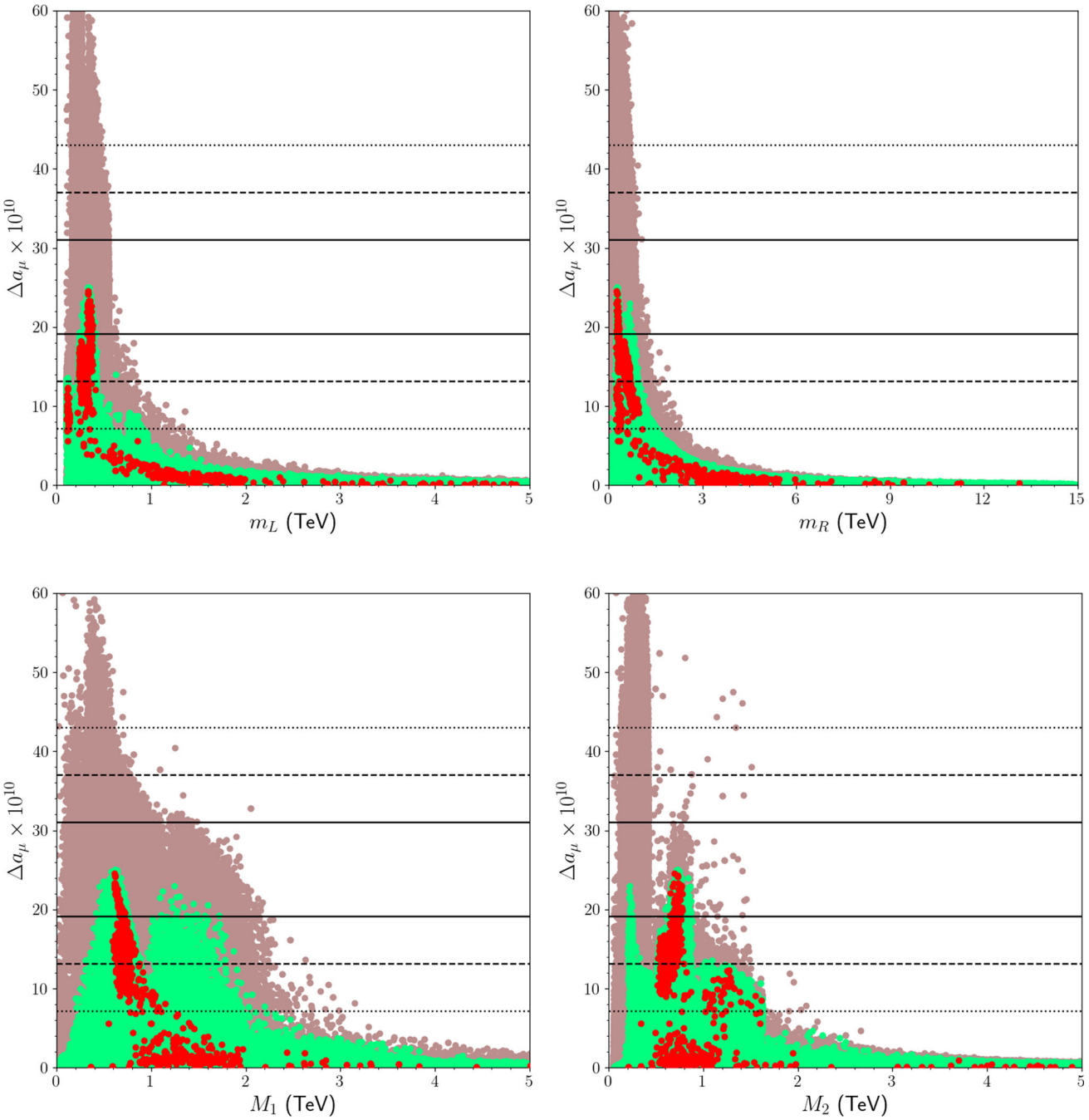


Fig. 2 Plots in the $\Delta a_\mu - m_L$, $\Delta a_\mu - m_R$, $\Delta a_\mu - M_1$ and $\Delta a_\mu - M_2$ planes. All solutions are compatible with the REWSB and LSP neutralino conditions. The green points are allowed by the mass bounds and constraints from rare B-meson decays. The red points form a subset of green and they satisfy the Planck measurements on the relic density of LSP neutralino within 5σ. The horizontal solid, dashed and dotted lines bound the regions which accommodate the muon $g-2$ resolution within 1σ, 2σ and 3σ respectively

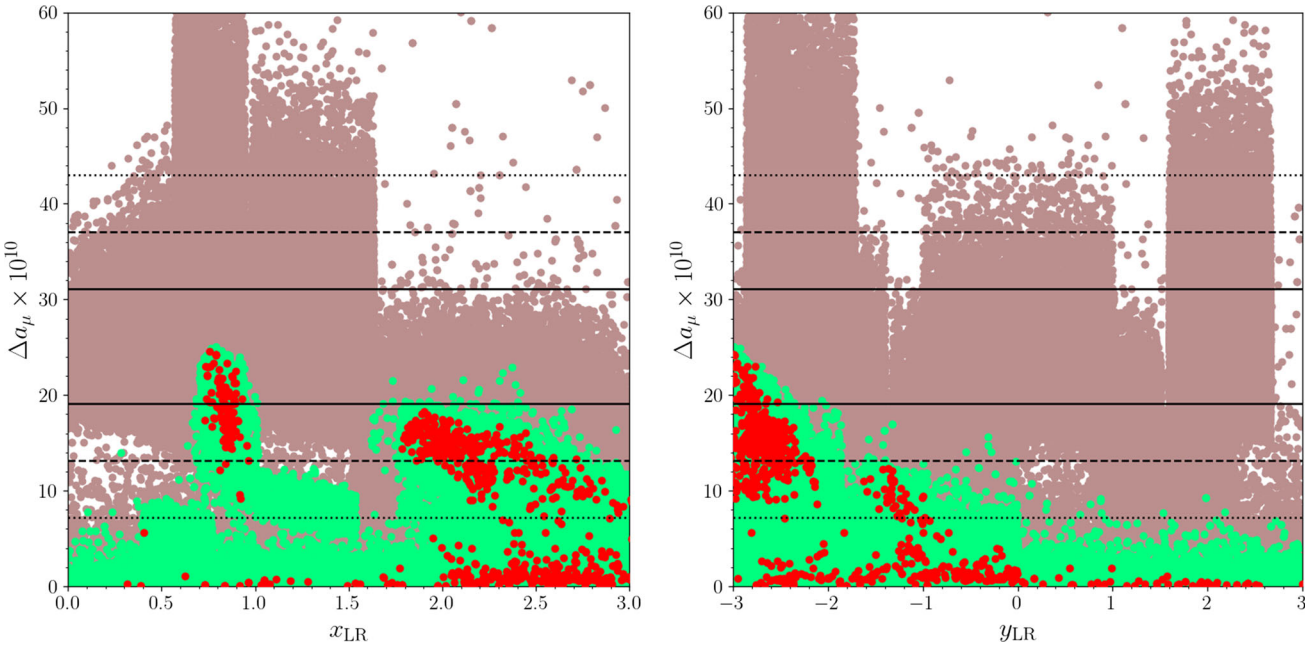


Fig. 3 LR breaking and muon $g-2$ implications in the $\Delta a_\mu - x_{LR}$ and $\Delta a_\mu - y_{LR}$ planes. The meanings of colors and horizontal lines are the same as in Fig. 2

symmetric muon $g-2$ contributions on $\tan\beta$ can be seen in the $\Delta a_\mu - \tan\beta$ plane, the mass bounds and consistent B-meson decays (green) can allow muon $g-2$ solutions within 2σ only in the regions with $\tan\beta \lesssim 22$. Requiring the LSP to be a consistent DM candidate (red points) lowers this bound further to $\tan\beta \lesssim 17$. This observation yields a strong tension between the experimental constraints and supersymmetric muon $g-2$ contributions, since the latter are enhanced with large $\tan\beta$. Even though we present the results on the parameter $\tan\beta$ in terms of consistency with all the constraints employed in our analyses, the main negative impact comes from the constraint on the Higgs boson mass, which is shown in the bottom-left panel of Fig. 4.

As previously discussed, the loop contributions to the Higgs boson mass from stops are suppressed for larger $\tan\beta$ values, and a relatively small A_0 cannot compensate this suppression. Although it is possible to find models compatible with muon $g-2$ within 2σ and a Higgs boson mass close to 125 GeV, most of the solutions favored by muon $g-2$ predict the Higgs mass below the experimental value. Despite the enhancement arising from the sbottom and stau as discussed in Eq. (2.5), for large $\tan\beta$ values, these contributions are relatively minor due to the restriction on $\mu\tan\beta$ from the vacuum stability requirement on the scalar potential [50–52]. Therefore, only models with a heavy stop can compensate the suppressed loop contribution to the Higgs boson mass. However, since the SUSY contribution to the muon $g-2$ problem restricts the SSB mass parameters, m_L $(m_R) \lesssim 400$ (1200) GeV, the low scale sparticle spectrum cannot involve such heavy stops. As a consequence, to solve the muon $g-2$ anomaly a combination of large $\tan\beta$ solutions with relatively large value of μ is needed. As shown in the $\Delta a_\mu - \mu$ plane in Fig. 4, the desired solutions are realized for $\mu \gtrsim 3.5$ TeV, but the magnitude of μ is also limited since it cannot exceed 6 TeV. Realizing such large values of μ needs larger ranges for the SSB masses at the GUT scale for the gauginos and/or supersymmetric scalar particles, which leads to a heavier mass spectrum in the electroweak sector. In this case, the loop suppression encoded in the function $F_{\rm N}$ in Eq. (2.3) dominates over the enhancement from large μ values.

We also display the impact from the Higgs boson mass on the mass spectrum, mixing between the stops, and the muon $g-2$ solutions in Fig. 5 with plots in the $m_h - m_{\tilde{t}_1}$, $m_h - m_{\tilde{b}_1}$, $m_{\tilde{t}_1} - m_{\tilde{g}}$ and $\Delta a_\mu - X_t/M_{\rm SUSY}$ planes, where $X_t = A_t - \mu\cot\beta$. All points are compatible with the REWSB and LSP neutralino conditions. Green points satisfy the mass bounds and constraints from rare B-meson decays. The orange points form a subset of green and are compatible with the muon $g-2$ measurements within 2σ. Red points, as a subset of orange, are allowed by the Planck measurements on relic abundance of LSP neutralino within 5σ. In the top planes, the Higgs boson mass constraint is not included, but it is shown with the horizontal dotted lines. In the $\Delta a_\mu - X_t/M_{\rm SUSY}$ plane the horizontal lines represent the ranges of the experimental measurements of muon $g-2$ as defined in Fig. 2. The top panels show that the squark masses should lie between about 5 and 8 TeV in order to be consis-

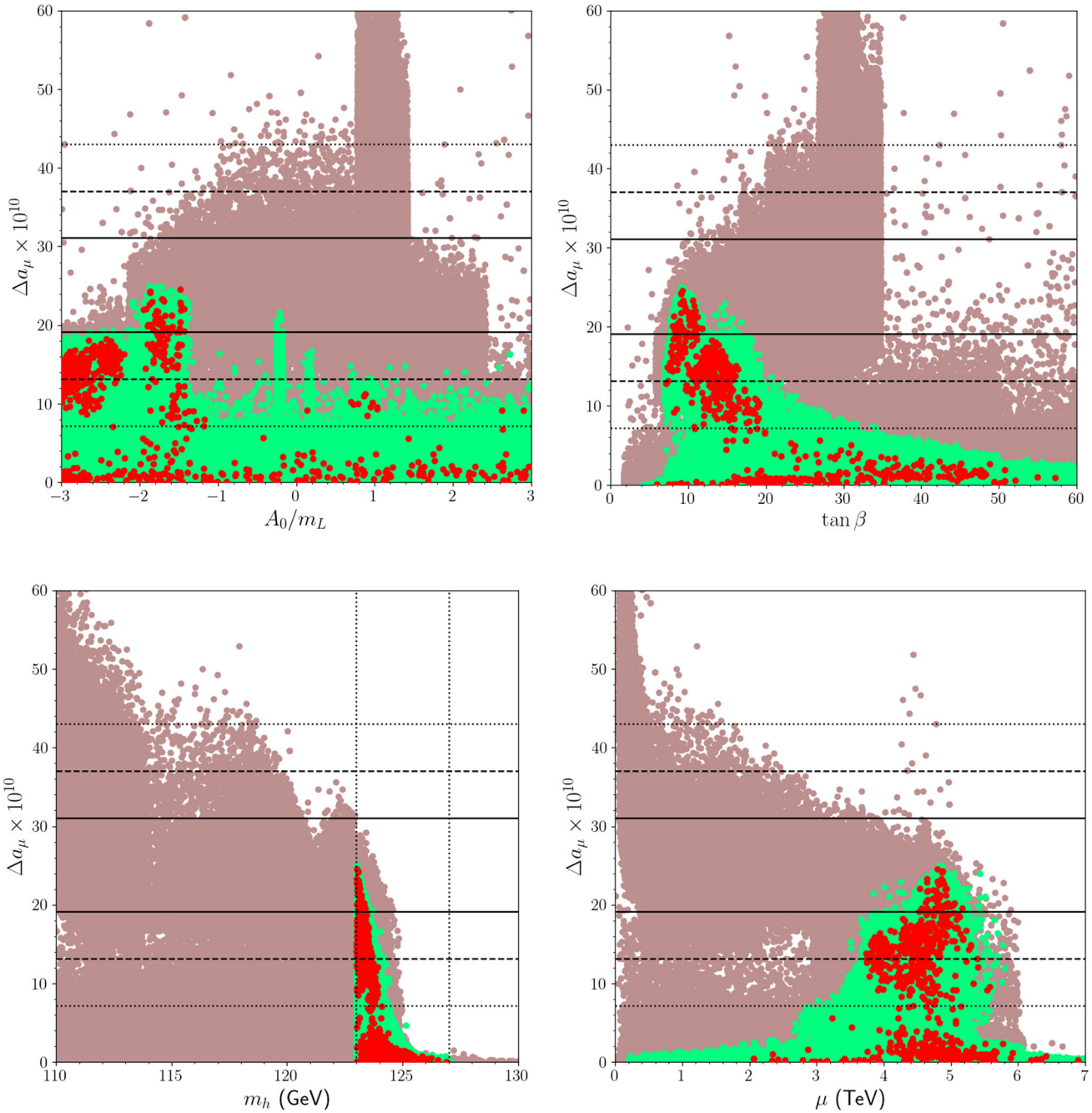


Fig. 4 Plots in the $\Delta a_\mu - A_0/m_L$, $\Delta a_\mu - \tan\beta$, $\Delta a_\mu - m_h$ and $\Delta a_\mu - \mu$ planes. The meanings of colors and horizontal lines are the same as in Fig. 2

tent with the Higgs boson mass. Considering the relatively lower bounds on m_L and m_R ($\lesssim 400, 800$ GeV respectively), the spectrum should involve heavy gluinos, which enhance the squark masses radiatively, and as shown in the $m_{\tilde{t}_1} - m_{\tilde{g}}$, the gluino is heavier than about 7 TeV for the muon $g-2$ solutions (orange and red). Finally, we display the mixing between the stops in the $\Delta a_\mu - X_t/M_{\rm SUSY}$ plane, and we observe a peak in the supersymmetric muon $g-2$ contributions at $X_t \sim M_{\rm SUSY}$, and compare with the stop masses $X_t \sim 5$ TeV. The maximal mixing between the stops requires $X_t \simeq 2M_{\rm SUSY}$ [93], and even though $X_t \sim M_{\rm SUSY}$ can be considered to be a relatively large mixing [28,94], one still needs heavy squarks in the spectrum in order to realize the observed Higgs boson mass.

Although the constraints mentioned above significantly shrink the region compatible with muon $g-2$, the solutions that survive these restrictions remain viable after further considerations. For instance, the relatively small values for $\tan\beta$

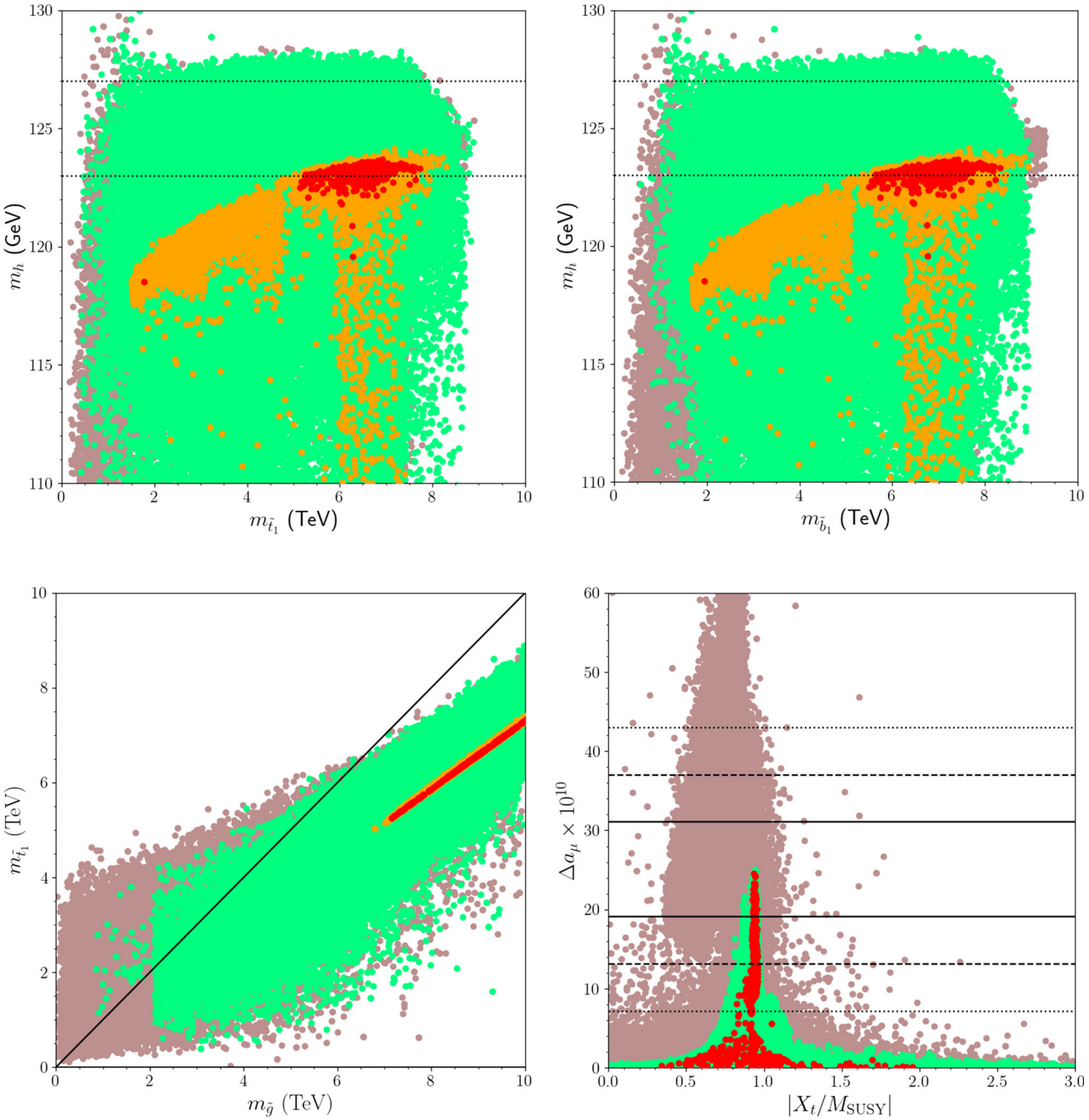


Fig. 5 The plots in the $m_h - m_{\tilde{t}_1}$, $m_h - m_{\tilde{b}_1}$, $m_{\tilde{t}_1} - m_{\tilde{g}}$ and $\Delta a_\mu - X_t/M_{\rm SUSY}$ planes, where $X_t = A_t - \mu \cot\beta$. All points are compatible with the REWSB and LSP neutralino conditions. Green points satisfy the mass bounds and constraints from rare B-meson decays. The orange points form a subset of green and compatible with the muon $g-2$ measurements within 2σ. Red points, as a subset of orange, are allowed by the Planck measurements on relic abundance of LSP neutralino within 5σ. In the top planes, the Higgs boson mass constraint is not included, but it is shown with the horizontal dotted lines. In the $\Delta a_\mu - X_t/M_{\rm SUSY}$ plane 1σ, 2σ and 3σ ranges of muon $g-2$ measurements are displayed by the horizontal solid, dashed and dotted lines, respectively

and A_0, and mildly large values for μ will help to find stable vacua in this region for the scalar potential. Figure 6 displays our results relevant to the Higgs boson mass and metastability condition on the vacuum with plots in the $m_L - \tan\beta$, $m_R - \tan\beta$, $\mu - \tan\beta$ and $\mu\tan\beta^{\max} - \mu\tan\beta$ planes. All points are compatible with REWSB and LSP neutralino conditions. Green points are allowed by the mass bounds and constraints from rare B-meson decays. The orange points form a subset of green, and they predict muon $g-2$ values within 2σ. The red points as a subset of orange, additionally yield the correct relic density of the LSP neutralino measured by the Planck satellite within 5σ uncertainty. $\mu\tan\beta^{\max}$ represents the possible maximum values of $\mu\tan\beta$ allowed by the metastability condition on the scalar potential, and the diagonal line in the $\mu\tan\beta^{\max} - \mu\tan\beta$ plane indicates the solutions for which $\mu\tan\beta = \mu\tan\beta^{\max}$. The top panels show the ranges of m_L and m_R favored by the muon $g-2$ solution within 2σ as $m_L \lesssim 400$ GeV and $m_R \lesssim 700$ GeV as stated before, and these ranges can yield a consistent Higgs boson mass if $\tan\beta \lesssim 17$. The $\mu - \tan\beta$ plane shows that the allowed values of μ lie between about 3.5–5.5 TeV, and its values tend to decrease with increasing $\tan\beta$. These lead to $\mu\tan\beta$ values only as large as about 100 TeV as shown in the $\mu\tan\beta^{\max} - \mu\tan\beta$ plane, where $\mu\tan\beta^{\max}$ is obtained by applying the metastability condition on the vacuum [52] to our data. As seen by comparing the solutions with respect to the diagonal line, only a few solutions that violate the metastability condition lie below the diagonal line (orange points). However, these solutions are already excluded by the Planck measurements on the DM relic density. The relic density constraint within 5σ bounds $\mu\tan\beta$ at about 70 TeV from above, and this is also more or less the bound imposed by the metastability condition. We should note here that we do not consider the quartic $|\tilde{\tau}_L\tilde{\tau}_R|^2$ term whose effects help to stabilize the vacuum and extend the metastability bound on $\mu\tan\beta$ to larger values [50]. Consequently, the solutions excluded by the metastability condition can still be available in further treatments on the vacuum stability.

In addition to the constraints discussed so far, the light sparticle spectrum has also been under active investigations by the current collider experiments at the LHC. We display some of these particles in Fig. 7, and the impact from LHC is expected to be improved during its Run3 phase, with plots in the $m_{\tilde{q}} - m_{\tilde{g}}$, $m_{\tilde{\tau}_L} - m_{\tilde{\tau}_R}$, $m_{\tilde{\mu}_L} - m_{\tilde{\mu}_R}$ and $m_{\tilde{\tau}_L} - m_{\tilde{\chi}_1^\pm}$ planes. The color coding is the same as used in Fig. 6, and the diagonal lines represent the degeneracy between the plotted masses. The green points with $m_{\tilde{g}} < 2$ TeV in the $m_{\tilde{q}} - m_{\tilde{g}}$ plane represent the NLSP gluino solutions for which $m_{\tilde{g}} \leq 1.1 m_{\tilde{\chi}_1^0}$. As stated in Eq. (3.2), the bound on the gluino mass can be lowered to about 800 GeV if it happens to be the NLSP, and these solutions predict the gluino–neutralino coannihilation scenario consistent with the LHC searches. However, due to the upper bound on the LSP neutralino mass of about 400 GeV, these NLSP gluino solutions are excluded by the desired muon $g-2$ solution. Even though we ensure the consistency with the bound on the gluino mass, the squarks might still happen to be inconsistently light due to the low values of m_L and m_R. The $m_{\tilde{q}} - m_{\tilde{g}}$ plane, where $\tilde{q}$ denotes the lightest squark in the first two families, shows that the gluino cannot be lighter than about 6 TeV. Such heavy gluinos are somewhat beyond the reach of the current and near future collider experiments, but they might become testable in collisions with a higher center of mass energy and luminosity [95]. Such heavy gluinos can also enhance the squark masses by contributing through RGEs, and results show that the squarks are always heavier than about 5 TeV in the muon $g-2$ compatible region.

In contrast to the colored particles, as shown in the $m_{\tilde{\tau}_L} - m_{\tilde{\tau}_R}$ plane, the staus cannot be heavier than about 500 GeV. Similar mass scales can be observed for the first two family sleptons in the $m_{\tilde{\mu}_L} - m_{\tilde{\mu}_R}$ plane. We display our results in the flavor basis for these particles because the LHC analyses are able to provide sensitive results for sleptons in these mass scales, through the chargino and neutralino decays involving the sleptons [23,24,96]. Such analyses can probe the first two family sleptons up to about 350 GeV, if they are mostly left-handed, while the chargino mass can be tested up to about 600 GeV in SUSY GUTs [25]. These bounds are expected to be lower when the stau is involved due to hadronic decays of τ-leptons in the final state.

5 Coannihilation scenarios and DM implications

In principle, the MSSM offers a variety of neutralino types - i.e. Bino, Wino and Higgsinos, and among them, the Higgsino can be found in the direct detection experiments because of its large scattering cross-sections with nuclei. However, the Planck measurements constrain its mass at about 700 GeV from below, and the current results of the direct detection experiments shift this bound even further to about 1 TeV (see, for instance, [80]). Similar results also hold for Wino-like DM as well, in which case the SUSY contributions to muon $g-2$ will be suppressed. In this context, the Bino can still provide viable DM solutions since its scattering cross-section is lower by a few orders of magnitude, which may become accessible in the ongoing and future direct detection experiments.

Since the muon $g-2$ compatible spectra involve relatively light sleptons, one can expect them to take part in the coannihilation scenarios. We display the masses of these sleptons and the LSP neutralino mass in Fig. 8 with plots in the $m_{\tilde{\mu}_1} - m_{\tilde{\chi}_1^0}$, $m_{\tilde{\mu}_2} - m_{\tilde{\chi}_1^0}$, $m_{\tilde{\tau}_1} - m_{\tilde{\chi}_1^0}$, $m_{\tilde{\nu}_1} - m_{\tilde{\chi}_1^0}$ planes. The color coding is the same as in Fig. 6. The diagonal lines show the mass degeneracy between the plotted SUSY par-

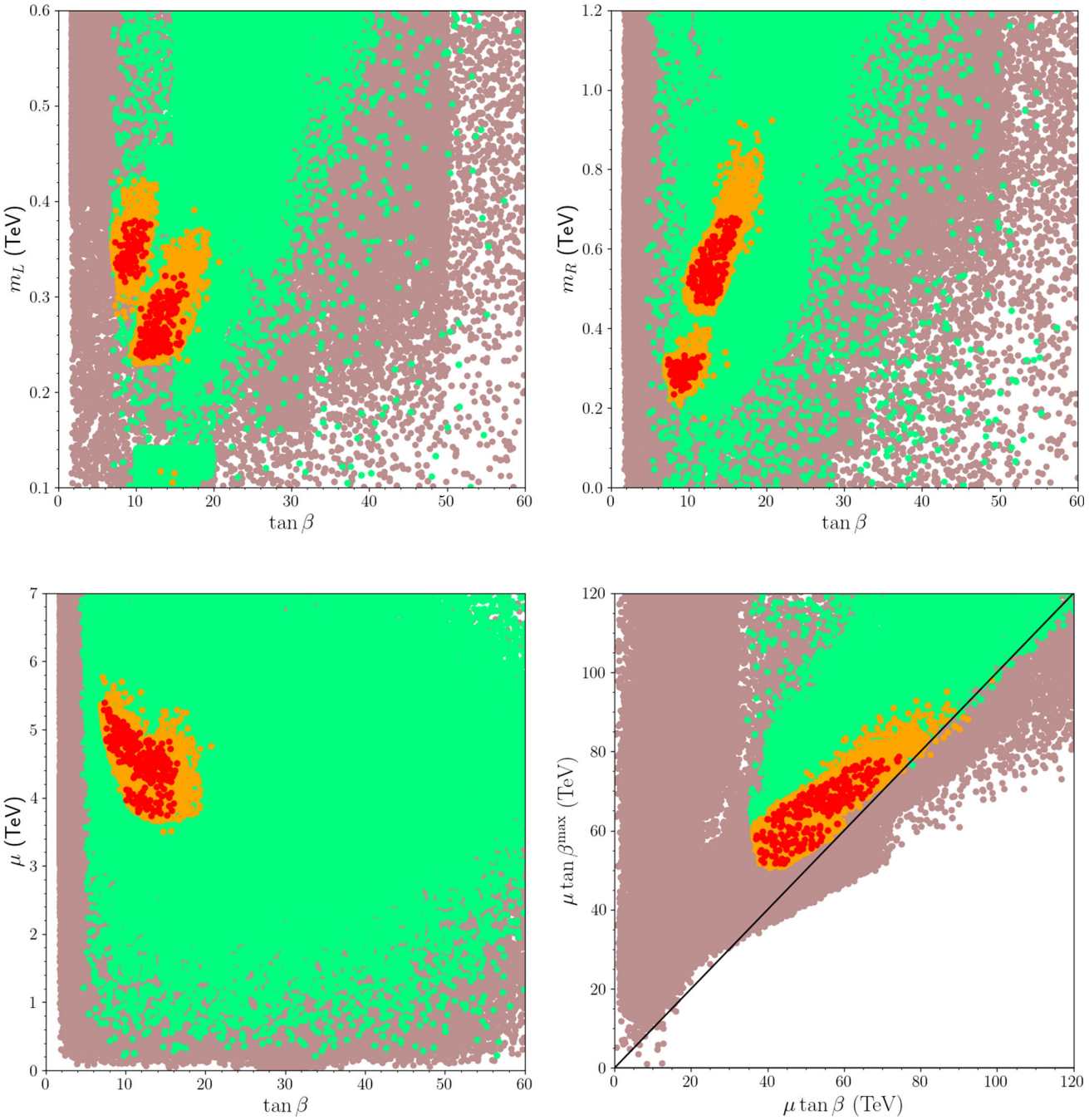


Fig. 6 The vacuum stability in $4-2-2$ with plots in the $m_L - \tan\beta$, $m_R - \tan\beta$, $\mu - \tan\beta$ and $\mu \tan\beta^{\max} - \mu \tan\beta$ planes. All points are compatible with the REWSB and LSP neutralino conditions. Green points are allowed by the mass bounds and constraints from rare B-meson decays. The orange points form a subset of green, and they accommodate the resolution to the muon $g-2$ discrepancy within 2σ. The red points as a subset of orange, additionally yield the correct relic density of the LSP neutralino measured by the Planck satellite within 5σ uncertainty. $\mu \tan\beta^{\max}$ represents the possible maximum values of $\mu \tan\beta$ allowed by the metastability condition on the scalar potential, and the the diagonal line in the $\mu \tan\beta^{\max} - \mu \tan\beta$ plane indicates the solutions for which $\mu \tan\beta = \mu \tan\beta^{\max}$

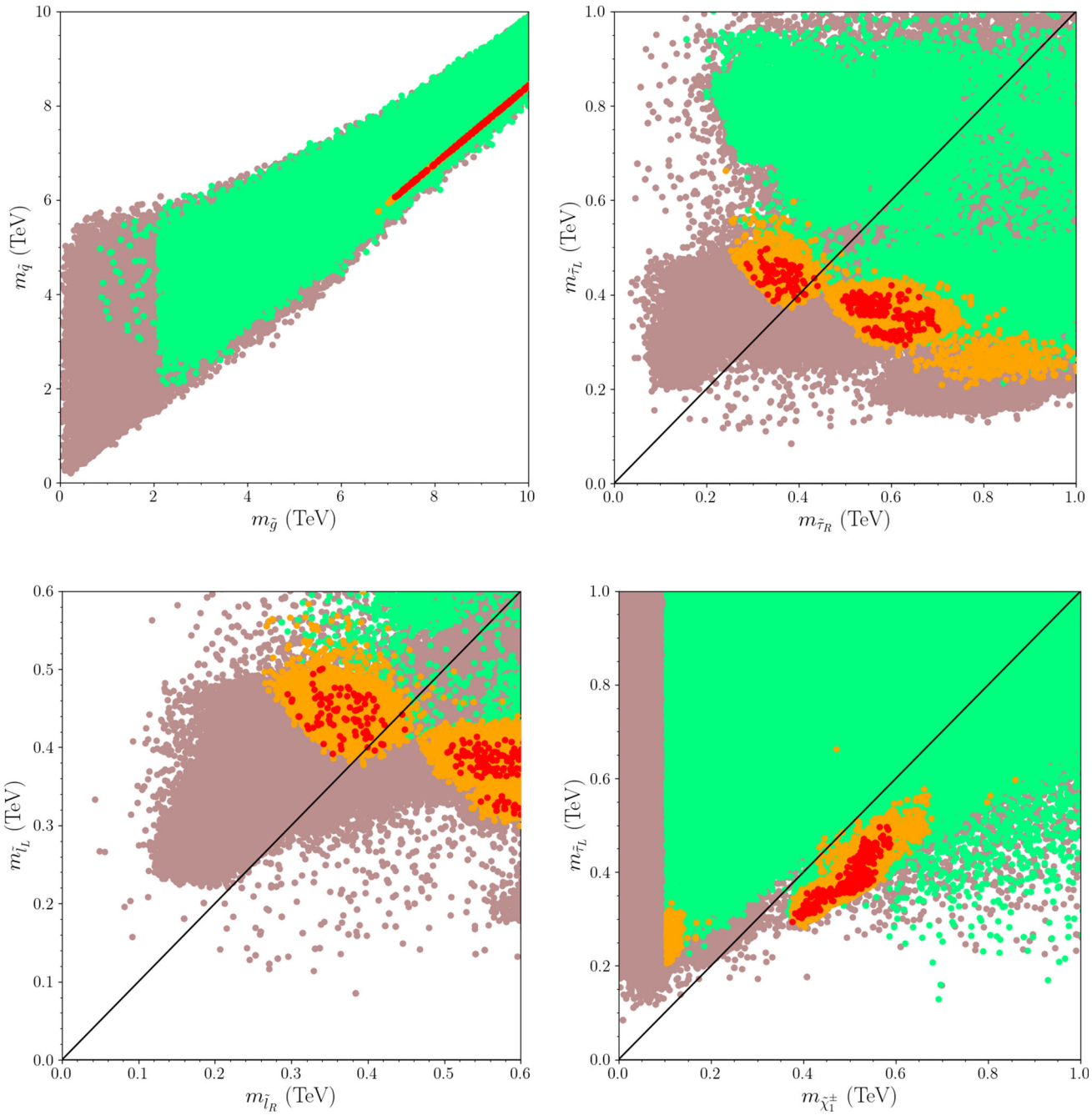


Fig. 7 Sparticle spectrum with plots in the $m_{\tilde{q}} - m_{\tilde{g}}$, $m_{\tilde{\tau}_L} - m_{\tilde{\tau}_R}$, $m_{\tilde{\mu}_L} - m_{\tilde{\mu}_R}$ and $m_{\tilde{\tau}_L} - m_{\tilde{\chi}_1^\pm}$ planes. The color coding is the same as used in Fig. 6. The diagonal lines represent the degeneracy between the plotted masses

ticles. The black curve in the $m_{\tilde{\tau}_1} - m_{\tilde{\chi}_1^0}$ plane displays the exclusion for the slepton masses with respect to the LSP neutralino masses from the analyses of the slepton pair production processes [97]. The main restriction from muon $g-2$ is on the smuon masses, and the desired region is realized for $m_{\tilde{\mu}_1} \lesssim 440$ GeV and $m_{\tilde{\mu}_2} \lesssim 800$ with the correct LSP relic density (red points), as seen in the top panels of Fig. 8. However, the mass differences between the LSP neutralino and smuons are larger than about 100 GeV, and thus they do not play a significant role in coannihilations. The mass differences between the LSP neutralino and staus are expected to be lower, and the plot in the $m_{\tilde{\tau}_1} - m_{\tilde{\chi}_1^0}$ plane shows that most of the solutions allowed by the Planck measurements and muon $g-2$ accumulate around the diagonal line where $m_{\tilde{\tau}_1} \simeq m_{\tilde{\chi}_1^0}$. The results show that the stau–neutralino coannihilation scenario can be realized for staus as light as about

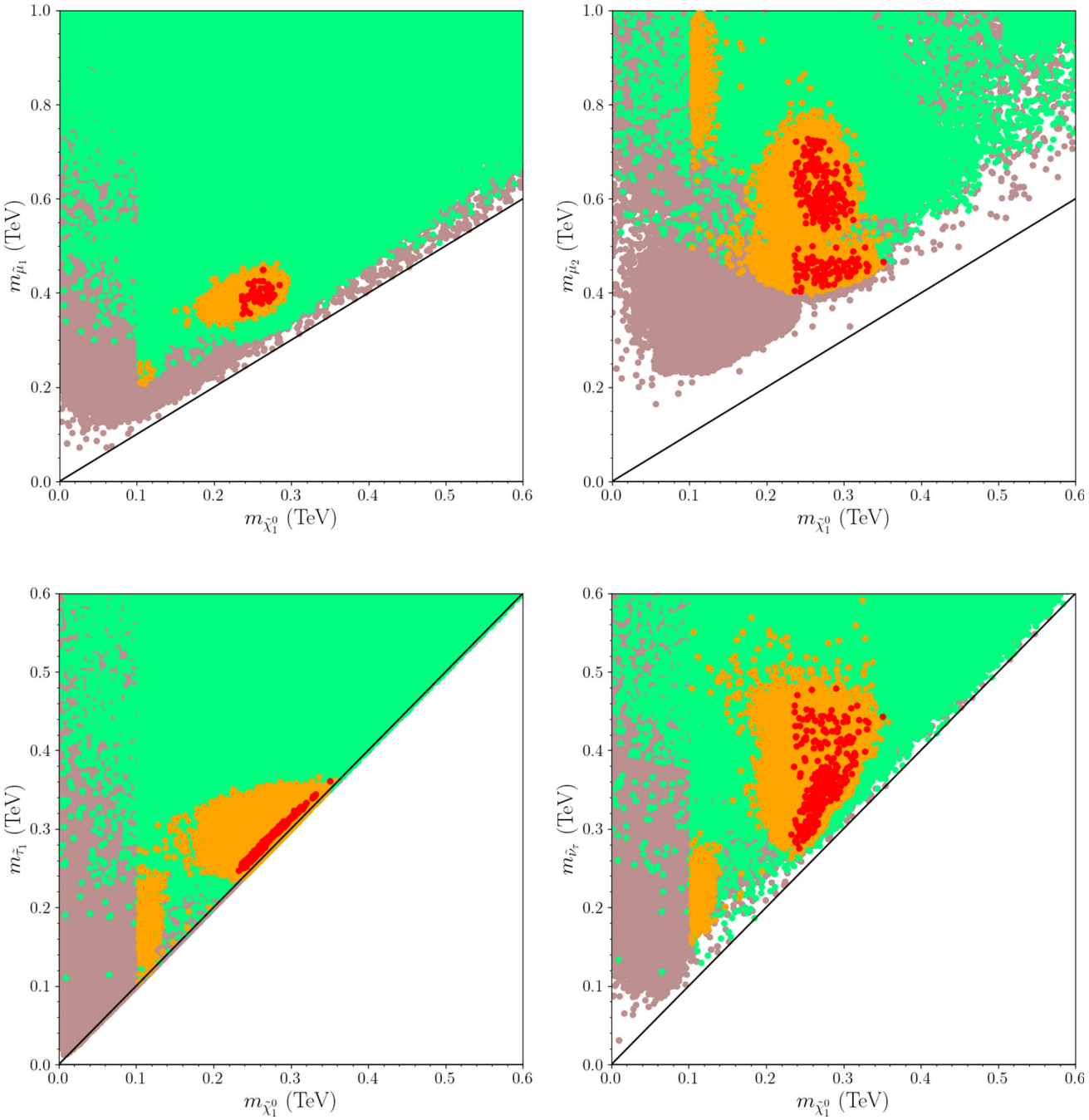


Fig. 8 Slepton spectrum with respect to the LSP neutralino mass in the $m_{\tilde{\mu}_1} - m_{\tilde{\chi}_1^0}, m_{\tilde{\mu}_2} - m_{\tilde{\chi}_1^0}, m_{\tilde{\tau}_1} - m_{\tilde{\chi}_1^0}, m_{\tilde{\nu}_1} - m_{\tilde{\chi}_1^0}$ planes. The color coding is the same as in Fig. 6. The diagonal lines show the mass degeneracy between the plotted SUSY particles. The black curve in the $m_{\tilde{\tau}_1} - m_{\tilde{\chi}_1^0}$ plane displays the exclusion for the slepton masses with respect to the LSP neutralino masses from the analyses of the slepton pair production processes [97]. The region below the black curve is excluded by these analyses.

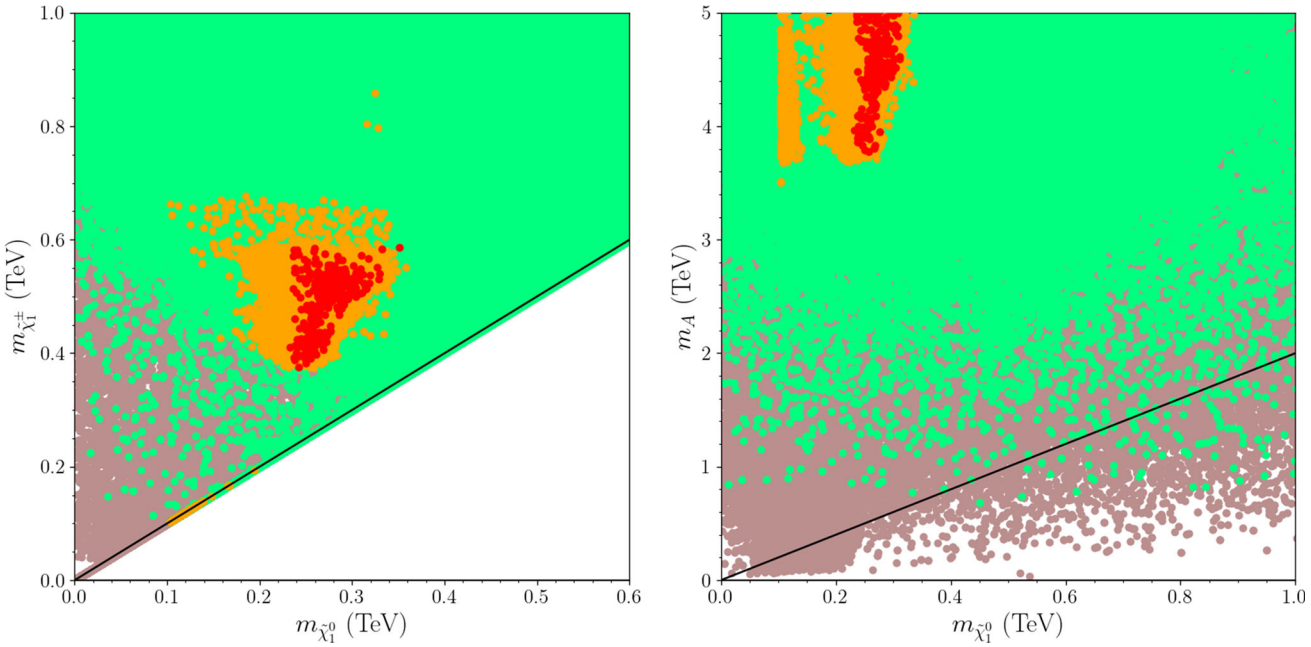


Fig. 9 Slepton spectrum with respect to the LSP neutralino mass in the $m_{\tilde{\chi}_1^\pm} - m_{\tilde{\chi}_1^0}$ and $m_A - m_{\tilde{\chi}_1^0}$ planes. The color coding is the same as in Fig. 6. The diagonal line in the left plane represents the solutions with $m_{\tilde{\chi}_1^\pm} = m_{\tilde{\chi}_1^0}$, and that in the right plane indicates the A-resonance solutions with $m_A = 2m_{\tilde{\chi}_1^0}$. The black, blue and magenta curves in the $m_{\tilde{\chi}_1^0} - m_{\tilde{\chi}_1^\pm}$ plane represent the bounds from the collider searches on the chargino–neutralino production with the final states of one lepton-pair of bottom quarks [98], no lepton [99] and a pair of bottom quarks [100], respectively. Each curve can exclude the regions below itself.

100 GeV, but the Planck measurements on the relic density of LSP neutralino exclude the solutions with $m_{\tilde{\tau}_1} \lesssim 250$ GeV. The muon $g-2$ solution together with the Planck measurements restrict the stau mass at about 350 GeV from above. This region also yields a sneutrino–neutralino coannihilation scenario for $m_{\tilde{\nu}_\tau} \gtrsim 250$ GeV, as shown in the $m_{\tilde{\nu}_1} - m_{\tilde{\chi}_1^0}$ plane. However, these coannihilations take part up to about 350 GeV sneutrino mass, since otherwise the mass difference between the sneutrino and LSP is more than 10% of the LSP neutralino mass (Fig. 9).

In addition to the stau and sneutrino, we also display our results for the chargino–neutralino coannihilation scenario and A-resonance solutions in Fig. 8 with plots in the $m_{\tilde{\chi}_1^\pm} - m_{\tilde{\chi}_1^0}$ and $m_A - m_{\tilde{\chi}_1^0}$ planes. The color coding is the same as in Fig. 5. The diagonal line in the left plane represents the solutions with $m_{\tilde{\chi}_1^\pm} = m_{\tilde{\chi}_1^0}$, and in the right plane it indicates the A-resonance solutions with $m_A = 2m_{\tilde{\chi}_1^0}$. We also display the bounds from collider searches on the chargino–neutralino production with the final states consisting of leptons and bottom quarks (black curve) [98], with no leptons (blue curve) [99], and a pair of bottom quarks (magenta curve) [100]. The results in the $m_{\tilde{\chi}_1^\pm} - m_{\tilde{\chi}_1^0}$ plane show no solution for the chargino–neutralino coannihilation scenario, if the LSP neutralino itself is the exclusive DM candidate with the correct relic density (red points). The chargino mass can lie between 400 and 600 GeV in this region. These mass scales can be impacted by the collider searches on the chargino–neutralino (or chargino-chargino) production and, as shown with the black and blue curves, the Run-II results can probe a few muon $g-2$ solutions consistent with the DM measurements. However, most of the solutions in red are slightly beyond the current exclusion curves, and one can expect these solutions to be probed during LHC Run-III. However, we also realize another region between about 100 and 200 GeV chargino mass, in which the chargino and LSP neutralino have almost degenerate masses. These solutions yield a considerable decrease in the relic density of LSP neutralino through chargino–neutralino coannihilation scenario. Comparing with the results displayed in the $m_{\tilde{\tau}_1} - m_{\tilde{\chi}_1^0}$ of Fig. 8, this region identifies chargino–neutralino and stau–neutralino coannihilation solutions simultaneously, which results in a very low relic density for the LSP neutralino that is incompatible with the Planck data. These solutions can be viable in scenarios which also include additional DM particles [101,102]. Finally, we also display our results in the $m_A - m_{\tilde{\chi}_1^0}$ where the diagonal line shows the the regions of A-resonance solutions. The CP-odd Higgs boson cannot be lighter than about 3.5 TeV in the spectra compatible with muon $g-2$, which is quite heavy for the A-resonance solutions.

In addition to the Planck measurements on the relic density of the LSP neutralino, the solutions discussed above can

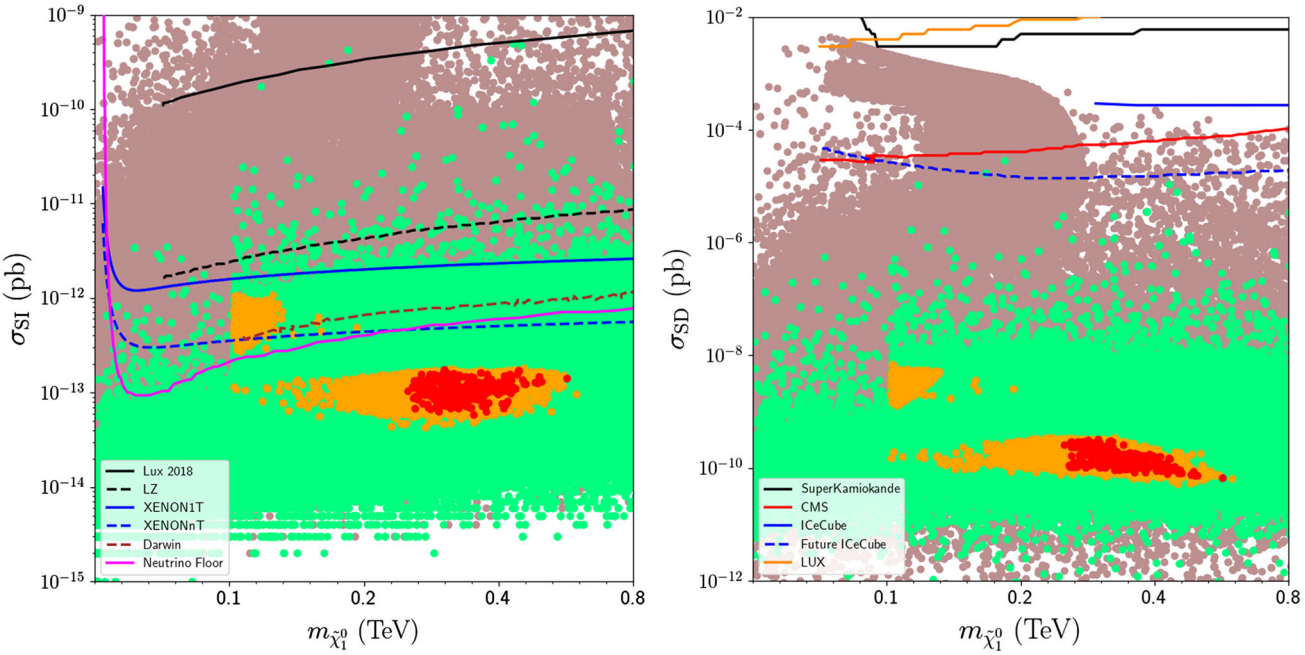


Fig. 10 Spin-independent (left) and spin-dependent (right) scattering cross-section in correlation with the LSP neutralino mass. The color coding is the same as in Fig. 6. The curves represent the current and projected exclusion curves from several direct detection DM experiments, whose color coding is given in the legend for each plane. The current exclusions are represented by the solid curves, and the dashed curves display the projected experimental sensitivity

be also probed in the direct detection experiments. We display our results in Fig. 10 for the spin-independent (left) and spin-dependent (right) scattering cross-sections versus the LSP neutralino mass. The color coding is the same as in Fig. 6. We also display the current and projected exclusion curves from several experiments, such as LUX, LZ [103], XENON [104] and DARWIN [105] for the spin-independent scattering cross-sections. The curves corresponding to the results of these experiments are listed in the legend of the $\sigma_{\rm SI} - m_{\tilde{\chi}_1^0}$ plane. The current exclusion limits are represented by the solid curves, and the dashed curves display the projected experimental sensitivities. We also include the neutrino floor, which is represented by the magenta curve. As discussed before, the Bino-like DM typically yields low scattering cross-sections, and the $\sigma_{\rm SI} - m_{\tilde{\chi}_1^0}$ plane shows that the solutions lie slightly below the most sensitive projection provided by XENONnT, and one may expect these solutions to be probed in the near future. However, these solutions fall below the neutrino floor, in which the relevant background is formed by solar and atmospheric neutrinos, and the DM detection in these regions requires significant statistics to overcome the neutrino background and the large uncertainties [106,107]. We also present our results for the case of spin-dependent scattering of LSP neutralino in the $\sigma_{\rm SD} - m_{\tilde{\chi}_1^0}$ plane together with some experimental results from SuperKamiokande [108], colliders [109], IceCube [110] and LUX [111] experiments. Our results indicate that some further upgrades in such experiments should be able to probe the solutions compatible with the latest muon $g-2$ experimental results (Fig. 11).

We also display results for the average annihilation cross-section of LSP neutralino, which can be tested in indirect detection experiments, in Fig. 10 in the $\langle\sigma v\rangle - m_{\tilde{\chi}_1^0}$ planes for the annihilation of the LSP neutralino into $\tau\bar{\tau}$ (left) and $l\bar{l}$ with $l = e, \mu$ (right). The color coding is the same as in Fig. 6. The dashed black curves in the planes represent the 6 year Pass 8 Limit from the Fermi-LAT measurements [112], and the dashed blue curve displays the bound on the thermal relic cross section [113]. We also include the 4 year Pass 7 Limit [114] with solid black curve, and the results including the contributions from the candidate dSphs [115] with dotted black line for the DM annihilation into $\tau\bar{\tau}$ in the left plane. Our results show that one can realize considerable average cross sections if the DM annihilates into a pair of leptons with $\langle\sigma v\rangle \sim 5\times10^{-28}$ cm^3 s^{-1} for $\tau\bar{\tau}$ and $\langle\sigma v\rangle \sim 5\times10^{-27}$ cm^3 s^{-1} for $l\bar{l}$, which are two to three orders of magnitude lower than the current sensitivity of the Fermi-LAT measurements. One can expect these solutions to be probed in the indirect detection experiments when the next upgraded results are revealed.

Finally, we exemplify our findings with six benchmark points listed in Table 2. The points selected are consistent with the mass bounds, the constraints from rare B-meson decays, Planck measurements within 5σ and muon $g-2$ solu-

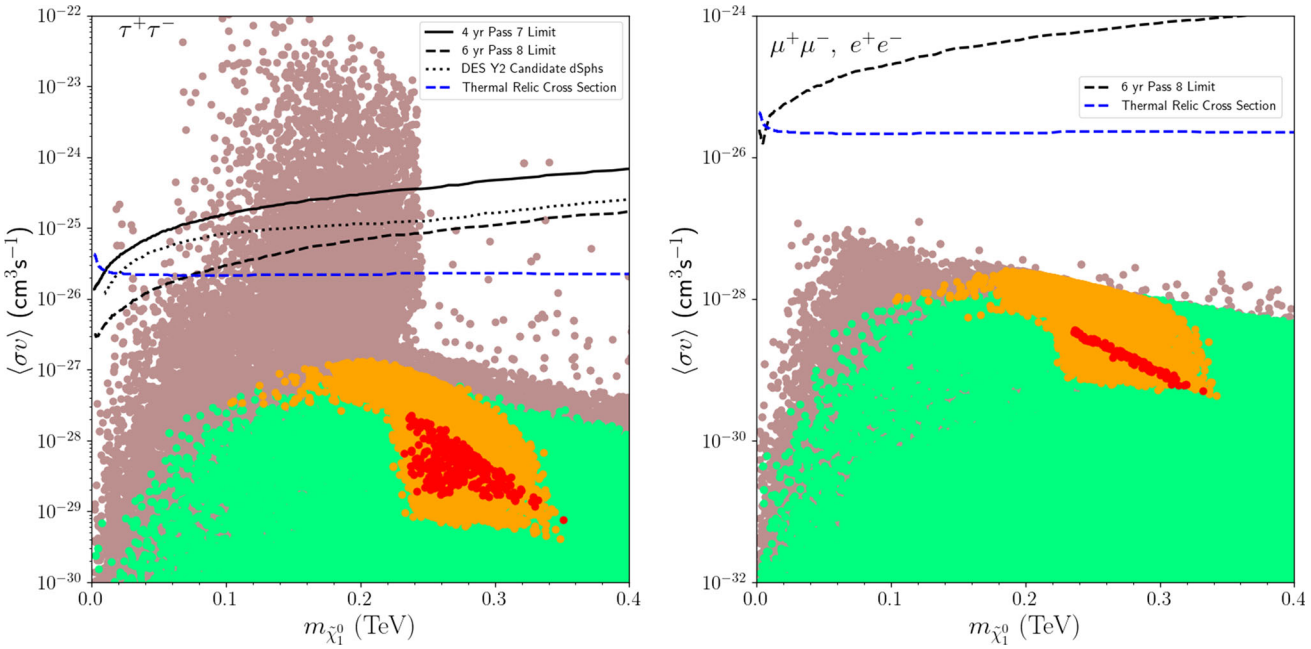


Fig. 11 The results for the indirect detection of DM in the $\langle\sigma v\rangle - m_{\tilde{\chi}_1^0}$ planes for the annihilation of the LSP neutralino into $\tau\bar{\tau}$ (left) and $l\bar{l}$ with $l = e, \mu$ (right). The color coding is the same as in Fig. 6. The dashed black curves in the planes represent the 6 year Pass 8 Limit from the Fermi-LAT measurements [112], while the dashed blue curve display the bound on the thermal relic cross section [113]. We also include the 4 year Pass 7 Limit [114] with solid black curve, and the results including the contributions from the candidate dSphs [115] with dotted black line for the DM annihilation into $\tau\bar{\tau}$ in the top-left plane

tion within $1\sigma - 2\sigma$. All masses are in GeV. Point 1 shows a solution that has muon $g-2$ value closest to its world average. Points 2 and 3 display solutions with the largest possible $\tan\beta$ consistent with the resolution of the muon $g-2$ anomaly within 1σ and 2σ respectively. Point 4 depicts a solution for the possible heaviest mass of the Higgs boson, and Point 5 refers to solutions with the smallest mass difference between $m_{\tilde{\chi}_1^0}$ and $m_{\tilde{\tau}_1}$. Point 6 exemplifies solutions for the chargino and LSP neutralino that are nearly degenerate in mass. The consistent relic density of LSP neutralino is achieved through the stau–neutralino and sneutrino–neutralino coannihilation scenarios as discussed before. All the points listed in Table 2 except Point 6, exemplify spectra in which the stau happens to be the NLSP (shown in italic), while the other slepton masses are lighter than about 450 GeV. On the other hand, the squarks mostly weigh more than about 7.2 TeV. The third family squarks can be slightly lighter ($m_{\tilde{t}_1} \gtrsim 5.6$ TeV), and the gluinos are heavier than about 8.5 TeV. Similarly, the muon $g-2$ solutions yield heavy Higgs bosons ($\gtrsim 4$ TeV) except the SM-like Higgs boson whose mass is around the edge allowed by the uncertainty. Even though they have spin-independent LSP neutralino scattering cross-sections lower than the current exclusion limits of the direct detection DM experiments, Points 1, 4, 5 and 6 predict a scattering cross-section on the order of 10^{-13} pb, which hopefully may be tested in the near future. The first five benchmark points in Table 2 display solutions with a Bino-like ($\gtrsim$ 99%) LSP neutralino, and Point 6 shows a Wino-like LSP neutralino, with a relic density well below the Planck measurements. Despite the low relic density, the latter solution is viable if an additional DM candidate is also present [101,102]. As we mentioned earlier, we used SPheno as a mass spectrum generator. However, it has been pointed out that the difference in the Higgs boson mass between SPheno and Softsusy can be up to about 2 GeV [83]. Therefore, we recomputed the mass spectrum of the benchmark points listed in Table 2 with Softsusy [116,117] linked to Himalaya three-loop corrections in calculating the Higgs boson mass. We found the difference in the Higgs boson mass prediction between these two numerical packages of about 0.6 GeV, with Softsusy yielding slightly heavier Higgs boson masses than SPheno. Furthermore, we observed that in the region of parameters that can fit muon $g-2$, characterized by SUSY particles below TeV and relatively small A_0 values, both codes provide comparable spectra.

Table 2 Benchmark points satisfy the mass bounds, the constraints from rare B-meson decays, Planck measurements within 5σ and muon $g-2$ solution within 2σ at most. All masses are in GeV. Point 1 shows a solution that has muon $g-2$ value closest to its world average. Points 2 and 3 display solutions with the possible largest tan β consistent with the muon $g-2$ solution within 1σ and 2σ respectively. Point 4 depicts a solution for the possible heaviest mass of the Higgs boson in the muon $g-2$ compatible region. Point 5 refers to solutions with the smallest difference in $m_{\tilde{\chi}_1^0}$ and $m_{\tilde{\tau}_1}$. Point 6 exemplifies a solution with nearly degenerate masses for the LSP neutralino, chargino and stau

	Point 1	Point 2	Point 3	Point 4	Point 5	Point 6
$m_{\widetilde{L}}$	335.319	375.605	311.513	377.107	330.994	361.925
M_1	616.148	672.019	633.965	767.804	787.614	1282.26
M_{2L}	731.027	747.131	603.037	721.392	698.554	327.194
M_3	4819.28	4920.39	4274.83	5067.11	4789.29	4505.82
$A_0/m_{\widetilde{L}}$	−1.87	−1.71	−2.93	−1.52	−1.52	0.73
tan β	9.08099	11.7627	16.1768	9.44659	7.63402	18.6131
x_{LR}	0.79	0.88	2.12	0.88	0.86	2.2
y_{LR}	−2.99	−2.89	−2.97	−2.91	−2.69	−2.65
$m_{\widetilde{R}}$	265.065	329.393	660.442	331.076	285.988	795.804
M_{2R}	−2185.94	−2160.23	−1793.28	−2098.4	−1880.17	−866.78
μ	4875.83	4951.28	4402.88	5098.57	4839.6	4493.68
$\Delta a_\mu \times 10^{10}$	**24.28**	19.8	15.05	16.99	14.91	13.92
m_h	123.07	123.142	123.031	**123.541**	123.03	123.215
m_H	4999.35	5061.57	4404.11	5222.41	5062.4	4498.81
m_A	4999.31	5061.55	4404.11	5222.38	5062.35	4498.81
$m_{H^\pm}$	4996.57	5058.82	4401.99	5219.5	5059.58	4496.11
$m_{\tilde{\chi}_1^0}, m_{\tilde{\chi}_2^0}$	*238*, 543	*263*, 557	*250*, 441	*305* , 532	*315*, 514	*194*, 530
$m_{\tilde{\chi}_3^0}, m_{\tilde{\chi}_4^0}$	4991,4992	5068, 5069	4504, 4505	5219, 5220	4956, 4957	4607, 4607
$m_{\tilde{\chi}_1^\pm}, m_{\tilde{\chi}_2^\pm}$	544, 4992	557, 5069	442, 4505	532, 5220	515, 4957	*195*, 4607
$m_{\tilde{g}}$	9549	9741	8555	10017	9501	9032
$m_{\tilde{u}_1}, m_{\tilde{u}_2}$	8049, 8050	8210, 8211	7231, 7259	8437, 8439	8012, 8012	7630, 7677
$m_{\tilde{t}_1}, m_{\tilde{t}_2}$	6979, 7525	7123, 7670	6267, 6724	7319, 7886	6945, 7492	6712, 7126
$m_{\tilde{d}_1}, m_{\tilde{d}_2}$	8051, 8055	8212, 8216	7231, 7262	8438, 8444	8012, 8018	7630, 7678
$m_{\tilde{b}_1}, m_{\tilde{b}_2}$	7518, 8031	7662, 8177	6713, 7196	7878, 8417	7484, 8001	7117, 7598
$m_{\tilde{\nu}_{e,\mu}}, m_{\tilde{\nu}_\tau}$	430, 418	459, 438	369, 331	451, 437	403, 394	293, 246
$m_{\tilde{e}_1,\tilde{\mu}_1}, m_{\tilde{e}_2,\tilde{\mu}_2}$	368, 437	447, 465	377, 703	445, 458	410, 446	303, 937
$m_{\tilde{\tau}_1}, m_{\tilde{\tau}_2}$	*255*, 484	*284*, 535	*268*, 690	*320*, 523	*325*, 489	*200*, 919
$\sigma_{SI}(pb)$	1.15×10^{-13}	7.7×10^{-n14}	6.7×10^{-14}	1.05×10^{-13}	1.71×10^{-13}	4.86×10^{-13}
$\sigma_{SD}(pb)$	1.05×10^{-10}	1.04×10^{-10}	1.69×10^{-10}	8.97×10^{-11}	1.06×10^{-10}	2.58×10^{-9}
Ωh^2	0.118	0.119	0.116	0.115	0.115	0.001

6 Conclusions

We consider a class of SUSY GUTs in which the $SO(10)$ breaks via $4-2-2$ to MSSM. We assume the $SO(10)$ breaking to $4-2-2$ happens through the VEV of a Higgs fields in the 210 dimensional representation that also breaks the LR symmetry. The GUT spectrum also involves 126 and $\overline{126}$ dimensional Higgs representations, whose VEVs break $4-2-2$ to the MSSM gauge group. With such a breaking mechanism the possible D-term contributions to the SSB scalar masses are canceled, but the absence of LR symmetry yields different SSB masses at $M_{\rm GUT}$ for the left and right-handed supersymmetric scalars, as well as leading to non-universal gaugino masses.

We confront the predictions of this class of SUSY models with the recent Fermilab measurement of the anomalous muon $g-2$. We found a region of parameter space such that the model prediction agress within 1–2σ of experimental result. This region restricts the masses of sleptons, neutralino and chargino to be lighter than about 1 TeV and a typical spectrum involves NLSP staus whose mass has an upper limit of about 400 GeV. The Planck measurements on the DM relic density restrict the stau mass from below as $m_{\tilde{\tau}} \gtrsim 250$ GeV. The masses of the first two charged slepton families are found

to be slightly heavier, namely $m_{\tilde{l}} \gtrsim 350$ GeV, where $\tilde{l} = \tilde{e}, \tilde{\mu}$. Even though the supersymmetric muon $g-2$ contributions depend on the chargino mass, values for the latter larger than about 900 GeV are still compatible with the experimental muon $g-2$ measurement within 2σ. On the other hand, the DM relic density constraint imposes an upper bound of about 600 GeV for the chargino mass. Chargino and sleptons masses may be further restricted by the current and Run3 experiments at LHC. However, the dominant right-handed chirality of the lighter sleptons suppress chargino decays, which is mostly Wino-like, into these relatively light sleptons.

In contrast to the sleptons, chargino and LSP neutralino, the other SUSY particles are heavy. The supersymmetric muon $g-2$ contributions are enhanced by the relatively large μ-term, and as a result, the Higgsino masses are of about 4 TeV or heavier, with similar mass scales for the additional scalars present in the MSSM. However, the mass prediction for the SM-like Higgs becomes low at large $\tan\beta$. This is due to the fact that the stop contributions to the Higgs boson mass decrease with $\tan\beta$, and a heavier SUSY mass spectrum is needed to compensate this suppression. Therefore, considering the $\tan\beta$ enhancement in the supersymmetric contributions to muon $g-2$, there exists a significant tension between the muon $g-2$ resolution and the Higgs boson mass constraint. We find that the two requirements cannot satisfy the experimental results if $\tan\beta \gtrsim 17$. We also discussed vacuum stability which is easily satisfied for low $\tan\beta$ values. Indeed, we find that a small portion of the parameter space that violates the metastability condition on the scalar potential is already excluded by the DM relic density constraint.

The solution of the muon $g-2$ discrepancy within 2σ imposes an upper limit of about 350 GeV on the LSP neutralino mass. The LSP neutralino is pre-dominantly a Bino, with the lighter chargino mostly a Wino. Even though Bino-like DM typically yields a large relic density, its density can be lowered through coannihilation and annihilation processes, and the light sleptons in the spectrum are suitable for such coannihilation processes. The stau–neutralino coannihilation dominantes in reducing the LSP neutralino density, and snuetrino–neutralino coannihilation provides minor contributions for realizing the correct relic density of LSP neutralino. In this context, imposing the Planck measurements on the relic abundance of LSP neutralino on the muon $g-2$ compatible region result in an upper bound on the stau mass, $m_{\tilde{\tau}_1} \lesssim 360$ GeV. Even though the current LHC analyses [118,119] constrain severely the light slepton masses, the results from these analyses are crucially sensitive to the mass difference between the NLSP and LSP. If the mass difference is below 80 GeV [120,121], the possible signal processes involve soft tau leptons in their final states, which significantly raise the uncertainty in the experimental analyses due to relatively lower sensitivity of the detectors to tau lepton and large QCD background [122]. In our model the mass difference between the stau and LSP neutralino is not greater than about 15 GeV in the stau–neutralino coannihilation region, and therefore the solutions we found remain intact. In addition, we identify a region with both chargino–neutralino and stau–neutralino coannihilations where the resultant relic density becomes lower than the current measurements of the Planck satellite.

Despite its low scattering cross-section, a Bino-like DM can provide compelling predictions since the current sensitivity of the direct DM detection experiments has improved significantly. Our solutions predict a spin-independent scattering cross-sections on the order of 10^{-13} pb, which is only slightly lower than the projected sensitivity of the XENON experiment and hopefully can be tested in the near future. We display results for the spin-dependent scattering of DM which lie well below the current and projected experimental sensitivities. We exemplify our findings using six benchmark points.

Acknowledgements This work is supported in part by the United States Department of Energy grant DE-SC0013880 (QS and AT). The research of MEG and CSU is supported in part by the Spanish MICINN, under grant PID2019-107844GB-C22. We acknowledge Information Technologies (IT) resources at the University Of Delaware, specifically the high performance computing resources for the calculation of results presented in this paper.

Data Availability Statement This manuscript has no associated data or the data will not be deposited. [Authors' comment: The data used in this article is generated through the theoretical calculations by employing publicly available numerical packages, and can be reproducible by anyone through the description provided in the article.]

Open Access This article is licensed under a Creative Commons Attribution 4.0 International License, which permits use, sharing, adaptation, distribution and reproduction in any medium or format, as long as you give appropriate credit to the original author(s) and the source, provide a link to the Creative Commons licence, and indicate if changes were made. The images or other third party material in this article are included in the article's Creative Commons licence, unless indicated otherwise in a credit line to the material. If material is not included in the article's Creative Commons licence and your intended use is not permitted by statutory regulation or exceeds the permitted use, you will need to obtain permission directly from the copyright holder. To view a copy of this licence, visit http://creativecommons.org/licenses/by/4.0/.
Funded by SCOAP[3].

References

1. Muon g-2 Collaboration, Measurement of the positive muon anomalous magnetic moment to 0.46 ppm. Phys. Rev. Lett. **126**, 141801 (2021). https://doi.org/10.1103/PhysRevLett.126.141801. arXiv:2104.03281
2. Muon g-2 Collaboration, Final report of the muon E821 anomalous magnetic moment measurement at BNL. Phys. Rev. D **73**,

072003 (2006). https://doi.org/10.1103/PhysRevD.73.072003. arXiv:hep-ex/0602035
3. M. Davier, A. Hoecker, B. Malaescu, Z. Zhang, Reevaluation of the hadronic contributions to the muon g-2 and to alpha(MZ). Eur. Phys. J. C **71**, 1515 (2011). https://doi.org/10.1140/epjc/s10052-012-1874-8 arXiv:1010.4180
4. K. Hagiwara, R. Liao, A.D. Martin, D. Nomura, T. Teubner, $(g-2)_\mu$ and $\alpha(M_Z^2)$ re-evaluated using new precise data. J. Phys. G **38**, 085003 (2011). https://doi.org/10.1088/0954-3899/38/8/085003 arXiv:1105.3149
5. S. Borsanyi et al., Leading hadronic contribution to the muon magnetic moment from lattice QCD. Nature **593**, 51 (2021). https://doi.org/10.1038/s41586-021-03418-1 arXiv:2002.12347
6. M. Chakraborti, S. Heinemeyer, I. Saha, The new "MUON G-2" result and supersymmetry. arXiv:2104.03287
7. H. Baer, V. Barger, H. Serce, Anomalous muon magnetic moment, supersymmetry, naturalness, LHC search limits and the landscape. Phys. Lett. B **820**, 136480 (2021). https://doi.org/10.1016/j.physletb.2021.136480 arXiv:2104.07597
8. A. Aboubrahim, M. Klasen, P. Nath, What the Fermilab muon $g-2$ experiment tells us about discovering supersymmetry at high luminosity and high energy upgrades to the LHC. Phys. Rev. D **104**, 035039 (2021). https://doi.org/10.1103/PhysRevD.104.035039 arXiv:2104.03839
9. F. Wang, L. Wu, Y. Xiao, J.M. Yang, Y. Zhang, GUT-scale constrained SUSY in light of E989 muon g-2 measurement. arXiv:2104.03262
10. C. Han, M.L. López-Ibáñez, A. Melis, O. Vives, L. Wu, J.M. Yang, LFV and (g-2) in non-universal SUSY models with light higgsinos. JHEP **05**, 102 (2020). https://doi.org/10.1007/JHEP05(2020)102 arXiv:2003.06187
11. Z. Altın, O. Özdal, C.S. Un, Muon g-2 in an alternative quasi-Yukawa unification with a less fine-tuned seesaw mechanism. Phys. Rev. D **97**, 055007 (2018). https://doi.org/10.1103/PhysRevD.97.055007 arXiv:1703.00229
12. Z. Li, G.-L. Liu, F. Wang, J.M. Yang, Y. Zhang, Gluino-SUGRA scenarios in light of FNAL muon g-2 anomaly. JHEP **12**, 219 (2021). https://doi.org/10.1007/JHEP12(2021)219 arXiv:2106.04466
13. J. Ellis, J.L. Evans, N. Nagata, D.V. Nanopoulos, K.A. Olive, Flipped $\mathbf{g}_\mu - 2$. Eur. Phys. J. C **81**, 1079 (2021). https://doi.org/10.1140/epjc/s10052-021-09829-8 arXiv:2107.03025
14. P. Athron, C. Balázs, D.H.J. Jacob, W. Kotlarski, D. Stöckinger, H. Stöckinger-Kim, New physics explanations of a_μ in light of the FNAL muon g-2 measurement. JHEP **09**, 080 (2021). https://doi.org/10.1007/JHEP09(2021)080 arXiv:2104.03691
15. M. Chakraborti, L. Roszkowski, S. Trojanowski, GUT-constrained supersymmetry and dark matter in light of the new $(g-2)_\mu$ determination. JHEP **05**, 252 (2021). https://doi.org/10.1007/JHEP05(2021)252 arXiv:2104.04458
16. M. Endo, K. Hamaguchi, S. Iwamoto, T. Kitahara, Supersymmetric interpretation of the muon g − 2 anomaly. JHEP **07**, 075 (2021). https://doi.org/10.1007/JHEP07(2021)075 arXiv:2104.03217
17. S. Iwamoto, T.T. Yanagida, N. Yokozaki, Wino-Higgsino dark matter in MSSM from the g−2 anomaly. Phys. Lett. B **823**, 136768 (2021). https://doi.org/10.1016/j.physletb.2021.136768 arXiv:2104.03223
18. S. Baum, M. Carena, N.R. Shah, C.E.M. Wagner, The tiny (g-2) muon wobble from small-μ supersymmetry. JHEP **01**, 025 (2022). https://doi.org/10.1007/JHEP01(2022)025 arXiv:2104.03302
19. M. Frank, Y. Hiçyılmaz, S. Mondal, O. Özdal, C.S. Ün, Electron and muon magnetic moments and implications for dark matter and model characterisation in non-universal U(1)' supersymmetric models. JHEP **10**, 063 (2021). https://doi.org/10.1007/JHEP10(2021)063 arXiv:2107.04116
20. S. Heinemeyer, E. Kpatcha, I.N. Lara, D.E. López-Fogliani, C. Muñoz, N. Nagata, The new $(g-2)_\mu$ result and the $\mu\nu$SSM. Eur. Phys. J. C **81**, 802 (2021). https://doi.org/10.1140/epjc/s10052-021-09601-y. arXiv:2104.03294
21. ATLAS, CMS collaboration, Searches for gluinos and squarks. PoS **LHCP2019**, 168 (2019). https://doi.org/10.22323/1.350.0168. arXiv:1909.11753
22. ATLAS Collaboration, Search for squarks and gluinos in final states with same-sign leptons and jets using 139 fb^{-1} of data collected with the ATLAS detector. JHEP **06**, 046 (2020). https://doi.org/10.1007/JHEP06(2020)046. arXiv:1909.08457
23. CMS Collaboration, Search for electroweak production of charginos and neutralinos in multilepton final states in pp collision data at $\sqrt{s} = 13$ TeV, CMS-PAS-SUS-16-039
24. CMS Collaboration, Search for electroweak production of charginos and neutralinos in WH events in proton-proton collisions at $\sqrt{s} = 13$ TeV. JHEP **11**, 029 (2017). https://doi.org/10.1007/JHEP11(2017)029. arXiv:1706.09933
25. Q. Shafi, C.S. Ün, Sparticle spectroscopy at LHC-Run3 and LSP dark matter in light of muon g-2. arXiv:2107.04563
26. ATLAS Collaboration, Observation of a new particle in the search for the Standard Model Higgs boson with the ATLAS detector at the LHC. Phys. Lett. B **716**, 1 (2012). https://doi.org/10.1016/j.physletb.2012.08.020. arXiv:1207.7214
27. CMS Collaboration, Observation of a new boson with mass near 125 GeV in pp collisions at $\sqrt{s}$ = 7 and 8 TeV. JHEP **06**, 081 (2013). https://doi.org/10.1007/JHEP06(2013)081. arXiv:1303.4571
28. M. Carena, S. Gori, N.R. Shah, C.E.M. Wagner, A 125 GeV SM-like Higgs in the MSSM and the $\gamma\gamma$ rate. JHEP **03**, 014 (2012). https://doi.org/10.1007/JHEP03(2012)014 arXiv:1112.3336
29. J.C. Pati, A. Salam, Lepton number as the fourth color. Phys. Rev. D **10**, 275 (1974). https://doi.org/10.1103/PhysRevD.10.275
30. G. Lazarides, Q. Shafi, Comments on 'monopole charges in unified gauge theories'. Nucl. Phys. B **189**, 393 (1981)
31. T.W.B. Kibble, G. Lazarides, Q. Shafi, Strings in SO(10). Phys. Lett. B **113**, 237 (1982). https://doi.org/10.1016/0370-2693(82)90829-2
32. K.S. Babu, R.N. Mohapatra, Predictive neutrino spectrum in minimal SO(10) grand unification. Phys. Rev. Lett. **70**, 2845 (1993). https://doi.org/10.1103/PhysRevLett.70.2845 arXiv:hep-ph/9209215
33. G. Anderson, S. Raby, S. Dimopoulos, L.J. Hall, G.D. Starkman, A systematic SO(10) operator analysis for fermion masses. Phys. Rev. D **49**, 3660 (1994). https://doi.org/10.1103/PhysRevD.49.3660 arXiv:hep-ph/9308333
34. M. Drees, Intermediate scale symmetry breaking and the spectrum of super partners in superstring inspired supergravity models. Phys. Lett. B **181**, 279 (1986). https://doi.org/10.1016/0370-2693(86)90046-8
35. Y. Kawamura, H. Murayama, M. Yamaguchi, Probing symmetry breaking pattern using sfermion masses. Phys. Lett. B **324**, 52 (1994). https://doi.org/10.1016/0370-2693(94)00107-3 arXiv:hep-ph/9402254
36. C.F. Kolda, S.P. Martin, Low-energy supersymmetry with D term contributions to scalar masses. Phys. Rev. D **53**, 3871 (1996). https://doi.org/10.1103/PhysRevD.53.3871 arXiv:hep-ph/9503445
37. D.J. Miller, A.P. Morais, P.N. Pandita, Constraining grand unification using first and second generation sfermions. Phys. Rev. D **87**, 015007 (2013). https://doi.org/10.1103/PhysRevD.87.015007 arXiv:1208.5906
38. K.S. Babu, T. Enkhbat, B. Mukhopadhyaya, Split supersymmetry from anomalous U(1). Nucl. Phys. B **720**, 47 (2005). https://doi.org/10.1016/j.nuclphysb.2005.05.006 arXiv:hep-ph/0501079

39. T.W.B. Kibble, G. Lazarides, Q. Shafi, Walls bounded by strings. Phys. Rev. D **26**, 435 (1982). https://doi.org/10.1103/PhysRevD.26.435
40. G. Lazarides, Q. Shafi, Superconducting membranes. Phys. Lett. B **159**, 261 (1985). https://doi.org/10.1016/0370-2693(85)90246-1
41. K.S. Babu, B. Bajc, S. Saad, Yukawa sector of minimal SO(10) unification. JHEP **02**, 136 (2017). https://doi.org/10.1007/JHEP02(2017)136 arXiv:1612.04329
42. Super-Kamiokande Collaboration, Atmospheric neutrino oscillation analysis with sub-leading effects in Super-Kamiokande I, II, and III. Phys. Rev. D **81**, 092004 (2010). https://doi.org/10.1103/PhysRevD.81.092004. arXiv:1002.3471
43. C. Coriano, L. Delle Rose, C. Marzo, Stability constraints of the scalar potential in extensions of the Standard Model with TeV scale right handed neutrinos. Nucl. Part. Phys. Proc. **265–266**, 311 (2015). https://doi.org/10.1016/j.nuclphysbps.2015.06.078. arXiv:1411.7168
44. S. Khalil, H. Okada, TeV scale B-L extension of the standard model. Prog. Theor. Phys. Suppl. **180**, 35 (2010). https://doi.org/10.1143/PTPS.180.35
45. M. Abbas, S. Khalil, Neutrino masses, mixing and leptogenesis in TeV scale B - L extension of the standard model. JHEP **04**, 056 (2008). https://doi.org/10.1088/1126-6708/2008/04/056 arXiv:0707.0841
46. T. Moroi, The Muon anomalous magnetic dipole moment in the minimal supersymmetric standard model. Phys. Rev. D **53**, 6565 (1996). https://doi.org/10.1103/PhysRevD.53.6565, https://doi.org/10.1103/PhysRevD.56.4424. arXiv:hep-ph/9512396
47. S.P. Martin, J.D. Wells, Muon anomalous magnetic dipole moment in supersymmetric theories. Phys. Rev. D **64**, 035003 (2001). https://doi.org/10.1103/PhysRevD.64.035003 arXiv:hep-ph/0103067
48. G.F. Giudice, P. Paradisi, A. Strumia, A. Strumia, Correlation between the Higgs decay rate to two photons and the muon g - 2. JHEP **10**, 186 (2012). https://doi.org/10.1007/JHEP10(2012)186 arXiv:1207.6393
49. H. Fargnoli, C. Gnendiger, S. Paßehr, D. Stöckinger, H. Stöckinger-Kim, Two-loop corrections to the muon magnetic moment from fermion/sfermion loops in the MSSM: detailed results. JHEP **02**, 070 (2014). https://doi.org/10.1007/JHEP02(2014)070 arXiv:1311.1775
50. M. Carena, S. Gori, I. Low, N.R. Shah, C.E.M. Wagner, Vacuum stability and Higgs diphoton decays in the MSSM. JHEP **02**, 114 (2013). https://doi.org/10.1007/JHEP02(2013)114 arXiv:1211.6136
51. J. Hisano, S. Sugiyama, Charge-breaking constraints on left-right mixing of stau's. Phys. Lett. B **696**, 92 (2011). https://doi.org/10.1016/j.physletb.2010.12.013 arXiv:1011.0260
52. T. Kitahara, T. Yoshinaga, Stau with large mass difference and enhancement of the Higgs to diphoton decay rate in the MSSM. JHEP **05**, 035 (2013). https://doi.org/10.1007/JHEP05(2013)035 arXiv:1303.0461
53. W. Porod, SPheno, a program for calculating supersymmetric spectra, SUSY particle decays and SUSY particle production at e+ e− colliders. Comput. Phys. Commun. **153**, 275 (2003). https://doi.org/10.1016/S0010-4655(03)00222-4 arXiv:hep-ph/0301101
54. W. Porod, F. Staub, SPheno 3.1: extensions including flavour, CP-phases and models beyond the MSSM. Comput. Phys. Commun. **183**, 2458 (2012). https://doi.org/10.1016/j.cpc.2012.05.021. arXiv:1104.1573
55. F. Staub, SARAH, arXiv:0806.0538
56. F. Staub, Introduction to SARAH and related tools. PoS **CORFU2015**, 027 (2016). https://doi.org/10.22323/1.263.0027. arXiv:1509.07061
57. U. Ellwanger, C. Hugonie, Constraints from charge and color breaking minima in the (M+1)SSM. Phys. Lett. B **457**, 299 (1999). https://doi.org/10.1016/S0370-2693(99)00546-8 arXiv:hep-ph/9902401
58. J.E. Camargo-Molina, B. O'Leary, W. Porod, F. Staub, **Vevacious**: a tool for finding the global minima of one-loop effective potentials with many scalars. Eur. Phys. J. C **73**, 2588 (2013). https://doi.org/10.1140/epjc/s10052-013-2588-2 arXiv:1307.1477
59. J.E. Camargo-Molina, B. O'Leary, W. Porod, F. Staub, Stability of the CMSSM against sfermion VEVs. JHEP **12**, 103 (2013). https://doi.org/10.1007/JHEP12(2013)103 arXiv:1309.7212
60. G. Belanger, F. Boudjema, A. Pukhov, R.K. Singh, Constraining the MSSM with universal gaugino masses and implication for searches at the LHC. JHEP **11**, 026 (2009). https://doi.org/10.1088/1126-6708/2009/11/026 arXiv:0906.5048
61. H. Baer, S. Kraml, S. Sekmen, H. Summy, Dark matter allowed scenarios for Yukawa-unified SO(10) SUSY GUTs. JHEP **03**, 056 (2008). https://doi.org/10.1088/1126-6708/2008/03/056 arXiv:0801.1831
62. R. Trotta, F. Feroz, M.P. Hobson, L. Roszkowski, R. Ruiz de Austri, The impact of priors and observables on parameter inferences in the constrained MSSM. JHEP **12**, 024 (2008). https://doi.org/10.1088/1126-6708/2008/12/024 arXiv:0809.3792
63. B.C. Allanach, A. Djouadi, J.L. Kneur, W. Porod, P. Slavich, Precise determination of the neutral Higgs boson masses in the MSSM. JHEP **09**, 044 (2004). https://doi.org/10.1088/1126-6708/2004/09/044 arXiv:hep-ph/0406166
64. D.M. Pierce, J.A. Bagger, K.T. Matchev, R.-J. Zhang, Precision corrections in the minimal supersymmetric standard model. Nucl. Phys. B **491**, 3 (1997). https://doi.org/10.1016/S0550-3213(96)00683-9 arXiv:hep-ph/9606211
65. A. Dedes, P. Slavich, Two loop corrections to radiative electroweak symmetry breaking in the MSSM. Nucl. Phys. B **657**, 333 (2003). https://doi.org/10.1016/S0550-3213(03)00173-1 arXiv:hep-ph/0212132
66. A. Dedes, G. Degrassi, P. Slavich, On the two loop Yukawa corrections to the MSSM Higgs boson masses at large tan beta. Nucl. Phys. B **672**, 144 (2003). https://doi.org/10.1016/j.nuclphysb.2003.08.033 arXiv:hep-ph/0305127
67. G. Bélanger, F. Boudjema, A. Goudelis, A. Pukhov, B. Zaldivar, micrOMEGAs5.0: freeze-in. Comput. Phys. Commun. **231**, 173 (2018). https://doi.org/10.1016/j.cpc.2018.04.027. arXiv:1801.03509
68. Particle Data Group Collaboration, Review of particle physics. Chin. Phys. C **38**, 090001 (2014). https://doi.org/10.1088/1674-1137/38/9/090001
69. LHCb Collaboration, First evidence for the decay $B_s^0 \to \mu^+\mu^-$. Phys. Rev. Lett. **110**, 021801 (2013). https://doi.org/10.1103/PhysRevLett.110.021801. arXiv:1211.2674
70. Heavy Flavor Averaging Group Collaboration, Averages of B-Hadron, C-Hadron, and tau-lepton properties as of early 2012. arXiv:1207.1158
71. Planck Collaboration, Planck 2018 results. I. Overview and the cosmological legacy of Planck. Astron. Astrophys. **641**, A1 (2020). https://doi.org/10.1051/0004-6361/201833880. arXiv:1807.06205
72. K.S. Babu, C.F. Kolda, Higgs mediated $B^0 \to \mu^+\mu^-$ in minimal supersymmetry. Phys. Rev. Lett. **84**, 228 (2000). https://doi.org/10.1103/PhysRevLett.84.228 arXiv:hep-ph/9909476
73. S.R. Choudhury, N. Gaur, Dileptonic decay of B(s) meson in SUSY models with large tan Beta. Phys. Lett. B **451**, 86 (1999). https://doi.org/10.1016/S0370-2693(99)00203-8 arXiv:hep-ph/9810307
74. S. Bertolini, F. Borzumati, A. Masiero, G. Ridolfi, Effects of supergravity induced electroweak breaking on rare B decays and

mixings. Nucl. Phys. B **353**, 591 (1991). https://doi.org/10.1016/0550-3213(91)90320-W
75. C. Greub, T. Hurth, B → X(s) gamma in the standard model. In *2nd International Conference on B Physics and CP Violation (BCONF 97)*, pp. 151–161, 7 (1997). https://doi.org/10.1142/9789814503952_0014. arXiv:hep-ph/9708214
76. K.G. Chetyrkin, M. Misiak, M. Munz, Weak radiative B meson decay beyond leading logarithms. Phys. Lett. B **400**, 206 (1997). https://doi.org/10.1016/S0370-2693(97)00324-9 arXiv:hep-ph/9612313
77. P. Bechtle, H.E. Haber, S. Heinemeyer, O. Stål, T. Stefaniak, G. Weiglein et al., The light and heavy Higgs interpretation of the MSSM. Eur. Phys. J. C **77**, 67 (2017). https://doi.org/10.1140/epjc/s10052-016-4584-9 arXiv:1608.00638
78. Y. Hiçyılmaz, L. Selbuz, L. Solmaz, C.S. Ün, Charged Higgs boson in MSSM and beyond. Phys. Rev. D **97**, 115041 (2018). https://doi.org/10.1103/PhysRevD.97.115041 arXiv:1711.07967
79. Y. Hiçyılmaz, L. Selbuz, L. Solmaz, C.S. Ün, Model characterization and dark matter in the secluded U(1)' model. Phys. Rev. D **105**, 055029 (2022). https://doi.org/10.1103/PhysRevD.105.055029 arXiv:2111.11930
80. S. Raza, Q. Shafi, C.S. Un, $b-\tau$ Yukawa unification in SUSY SU(5) with mirage mediation: LHC and dark matter implications. JHEP **05**, 046 (2019). https://doi.org/10.1007/JHEP05(2019)046 arXiv:1812.10128
81. M.E. Gómez, Q. Shafi, C.S. Un, Testing Yukawa unification at LHC Run-3 and HL-LHC. JHEP **07**, 096 (2020). https://doi.org/10.1007/JHEP07(2020)096 arXiv:2002.07517
82. A. Delgado, M. Quirós, Higgsino dark matter in the MSSM. Phys. Rev. D **103**, 015024 (2021). https://doi.org/10.1103/PhysRevD.103.015024 arXiv:2008.00954
83. H. Baer, V. Barger, D. Martinez, Comparison of SUSY spectra generators for natural SUSY and string landscape predictions. arXiv:2111.03096
84. P. Bergeron, P. Sandick, K. Sinha, Theoretical uncertainties in the calculation of supersymmetric dark matter observables. JHEP **05**, 113 (2018). https://doi.org/10.1007/JHEP05(2018)113 arXiv:1712.05491
85. CDF, D0 Collaboration, Combination of CDF and D0 results on the mass of the top quark. arXiv:0903.2503
86. I. Gogoladze, Q. Shafi, C.S. Un, Higgs boson mass from t-b-τ Yukawa unification. JHEP **08**, 028 (2012). https://doi.org/10.1007/JHEP08(2012)028 arXiv:1112.2206
87. M. Adeel Ajaib, I. Gogoladze, Q. Shafi, C.S. Un, A predictive Yukawa unified SO(10) model: Higgs and sparticle masses. JHEP **07**, 139 (2013). https://doi.org/10.1007/JHEP07(2013)139. arXiv:1303.6964
88. G. Degrassi, S. Heinemeyer, W. Hollik, P. Slavich, G. Weiglein, Towards high precision predictions for the MSSM Higgs sector. Eur. Phys. J. C **28**, 133 (2003). https://doi.org/10.1140/epjc/s2003-01152-2 arXiv:hep-ph/0212020
89. H. Bahl, S. Heinemeyer, W. Hollik, G. Weiglein, Theoretical uncertainties in the MSSM Higgs boson mass calculation. Eur. Phys. J. C **80**, 497 (2020). https://doi.org/10.1140/epjc/s10052-020-8079-3 arXiv:1912.04199
90. E. Bagnaschi, J. Pardo Vega, P. Slavich, Improved determination of the Higgs mass in the MSSM with heavy superpartners. Eur. Phys. J. C **77**, 334 (2017). https://doi.org/10.1140/epjc/s10052-017-4885-7. arXiv:1703.08166
91. P. Athron, J.-H. Park, T. Steudtner, D. Stöckinger, A. Voigt, Precise Higgs mass calculations in (non-)minimal supersymmetry at both high and low scales. JHEP **01**, 079 (2017). https://doi.org/10.1007/JHEP01(2017)079 arXiv:1609.00371
92. P. Drechsel, R. Gröber, S. Heinemeyer, M.M. Muhlleitner, H. Rzehak, G. Weiglein, Higgs-boson masses and mixing matrices in the NMSSM: analysis of on-shell calculations. Eur. Phys. J. C **77**, 366 (2017). https://doi.org/10.1140/epjc/s10052-017-4932-4 arXiv:1612.07681
93. F. Brummer, S. Kraml, S. Kulkarni, Anatomy of maximal stop mixing in the MSSM. JHEP **08**, 089 (2012). https://doi.org/10.1007/JHEP08(2012)089 arXiv:1204.5977
94. A. Djouadi, The anatomy of electro-weak symmetry breaking. II. The Higgs bosons in the minimal supersymmetric model. Phys. Rep. **459**, 1 (2008). https://doi.org/10.1016/j.physrep.2007.10.005. arXiv:hep-ph/0503173
95. Z. Altın, A. Çiçi, Z. Kırca, Q. Shafi, C.S. Ün, Gluino search with stop and top in nonuniversal gaugino mass models at LHC and future colliders. arXiv:1910.01457
96. ATLAS Collaboration, Search for electroweak production of supersymmetric particles in final states with two or three leptons at $\sqrt{s} = 13$ TeV with the ATLAS detector. Eur. Phys. J. C **78**, 995 (2018). https://doi.org/10.1140/epjc/s10052-018-6423-7. arXiv:1803.02762
97. ATLAS Collaboration, Search for electroweak production of charginos and sleptons decaying into final states with two leptons and missing transverse momentum in $\sqrt{s} = 13$ TeV pp collisions using the ATLAS detector. Eur. Phys. J. C **80**, 123 (2020). https://doi.org/10.1140/epjc/s10052-019-7594-6. arXiv:1908.08215
98. ATLAS Collaboration, Search for direct production of electroweakinos in final states with one lepton, missing transverse momentum and a Higgs boson decaying into two b-jets in pp collisions at $\sqrt{s} = 13$ TeV with the ATLAS detector. Eur. Phys. J. C **80**, 691 (2020). https://doi.org/10.1140/epjc/s10052-020-8050-3. arXiv:1909.09226
99. ATLAS Collaboration, Search for charginos and neutralinos in final states with two boosted hadronically decaying bosons and missing transverse momentum in pp collisions at $\sqrt{s} = 13$ TeV with the ATLAS detector, ATLAS-CONF-2021-022
100. ATLAS Collaboration, Search for chargino and neutralino production in final states with a Higgs boson and missing transverse momentum at $\sqrt{s} = 13$ TeV with the ATLAS detector. Phys. Rev. D **100**, 012006 (2019). https://doi.org/10.1103/PhysRevD.100.012006. arXiv:1812.09432
101. H. Baer, I. Gogoladze, A. Mustafayev, S. Raza, Q. Shafi, Sparticle mass spectra from SU(5) SUSY GUT models with $b-\tau$ Yukawa coupling unification. JHEP **03**, 047 (2012). https://doi.org/10.1007/JHEP03(2012)047 arXiv:1201.4412
102. T. Li, D.V. Nanopoulos, S. Raza, X.-C. Wang, A realistic intersecting D6-brane model after the first LHC run. JHEP **08**, 128 (2014). https://doi.org/10.1007/JHEP08(2014)128 arXiv:1406.5574
103. LUX-ZEPLIN Collaboration, Projected WIMP sensitivity of the LUX-ZEPLIN dark matter experiment. Phys. Rev. D **101**, 052002 (2020). https://doi.org/10.1103/PhysRevD.101.052002. arXiv:1802.06039
104. XENON Collaboration, Projected WIMP sensitivity of the XENONnT dark matter experiment. JCAP **2011**, 031 (2020). https://doi.org/10.1088/1475-7516/2020/11/031. arXiv:2007.08796
105. DARWIN Collaboration, DARWIN: towards the ultimate dark matter detector. JCAP **1611**, 017 (2016). https://doi.org/10.1088/1475-7516/2016/11/017. arXiv:1606.07001
106. C.A.J. O'Hare, New definition of the neutrino floor for direct dark matter searches. Phys. Rev. Lett. **127**, 251802 (2021). https://doi.org/10.1103/PhysRevLett.127.251802 arXiv:2109.03116
107. G.B. Gelmini, V. Takhistov, S.J. Witte, Casting a wide signal net with future direct dark matter detection experiments. JCAP **07**, 009 (2018). https://doi.org/10.1088/1475-7516/2018/07/009 arXiv:1804.01638
108. Super-Kamiokande Collaboration, An indirect search for WIMPs in the sun using 3109.6 days of upward-going muons in super-Kamiokande. Astrophys. J. **742**, 78 (2011). https://doi.org/10.1088/0004-637X/742/2/78. arXiv:1108.3384

109. CMS Collaboration, Search for dark matter, extra dimensions, and unparticles in monojet events in proton–proton collisions at $\sqrt{s} = 8$ TeV. Eur. Phys. J. C **75**, 235 (2015). https://doi.org/10.1140/epjc/s10052-015-3451-4. arXiv:1408.3583
110. IceCube Collaboration, Limits on a muon flux from neutralino annihilations in the Sun with the IceCube 22-string detector. Phys. Rev. Lett. **102**, 201302 (2009). https://doi.org/10.1103/PhysRevLett.102.201302. arXiv:0902.2460
111. LUX Collaboration, Results on the spin-dependent scattering of weakly interacting massive particles on nucleons from the Run 3 data of the LUX experiment. Phys. Rev. Lett. **116**, 161302 (2016). https://doi.org/10.1103/PhysRevLett.116.161302. arXiv:1602.03489
112. Fermi-LAT Collaboration, Searching for dark matter annihilation from Milky Way dwarf spheroidal galaxies with six years of fermi large area telescope data. Phys. Rev. Lett. **115**, 231301 (2015). https://doi.org/10.1103/PhysRevLett.115.231301. arXiv:1503.02641
113. G. Steigman, B. Dasgupta, J.F. Beacom, Precise Relic WIMP abundance and its impact on searches for dark matter annihilation. Phys. Rev. D **86**, 023506 (2012). https://doi.org/10.1103/PhysRevD.86.023506 arXiv:1204.3622
114. Fermi-LAT Collaboration, Dark matter constraints from observations of 25 Milky Way satellite galaxies with the fermi large area telescope. Phys. Rev. D **89**, 042001 (2014). https://doi.org/10.1103/PhysRevD.89.042001. arXiv:1310.0828
115. Fermi-LAT, DES Collaboration, Search for gamma-ray emission from DES dwarf spheroidal galaxy candidates with fermi-LAT data. Astrophys. J. Lett. **809**, L4 (2015). https://doi.org/10.1088/2041-8205/809/1/L4. arXiv:1503.02632
116. B.C. Allanach, SOFTSUSY: a program for calculating supersymmetric spectra. Comput. Phys. Commun. **143**, 305 (2002). https://doi.org/10.1016/S0010-4655(01)00460-X arXiv:hep-ph/0104145
117. B.C. Allanach, A. Bednyakov, R. Ruiz de Austri, Higher order corrections and unification in the minimal supersymmetric standard model: SOFTSUSY3.5. Comput. Phys. Commun. **189**, 192 (2015). https://doi.org/10.1016/j.cpc.2014.12.006. arXiv:1407.6130
118. ATLAS Collaboration, Search for electroweak production of supersymmetric particles in final states with two or three leptons at $\sqrt{s} = 13$ TeV with the ATLAS detector. Eur. Phys. J. C **78**, 995 (2018). https://doi.org/10.1140/epjc/s10052-018-6423-7. arXiv:1803.02762
119. CMS Collaboration, Search for supersymmetric partners of electrons and muons in proton–proton collisions at $\sqrt{s} = 13$ TeV. Phys. Lett. B **790**, 140 (2019). https://doi.org/10.1016/j.physletb.2019.01.005. arXiv:1806.05264
120. CMS Collaboration, Search for supersymmetry with a compressed mass spectrum in events with a soft τ lepton, a highly energetic jet, and large missing transverse momentum in proton-proton collisions at $\sqrt{s} =$ TeV. Phys. Rev. Lett. **124**, 041803 (2020). https://doi.org/10.1103/PhysRevLett.124.041803. arXiv:1910.01185
121. M. Chakraborti, S. Heinemeyer, I. Saha, Improved $(g-2)_\mu$ measurements and supersymmetry. Eur. Phys. J. C **80**, 984 (2020). https://doi.org/10.1140/epjc/s10052-020-08504-8 arXiv:2006.15157
122. CMS Collaboration, Search for direct pair production of supersymmetric partners to the τ lepton in proton–proton collisions at $\sqrt{s} = 13$ TeV. Eur. Phys. J. C **80**, 189 (2020). https://doi.org/10.1140/epjc/s10052-020-7739-7. arXiv:1907.13179